McGill University

Montreal, Quebec, Canada

Development of a 3D microenvironment for human bone metastasis

By Antone Nour

Division of Experimental Surgery

Faculty of Medicine

McGill University

Montreal

July 2021

A thesis submitted to McGill University in partial fulfillment of the requirements of the degree of Master of Science

©Antone Nour, 2021

TABLE OF CONTENTS

ABSTRACT

Bone is a dynamic tissue maintained through remodeling whereby it is constantly broken down and repaired through an equilibrium of osteoclast and osteoblast activity. However, when various cancers invade the bone, they disrupt this balance, leading to harmful bone structure and function changes. Radiotherapy, chemotherapy, and surgical resection are the main clinical approaches to bone metastases. Studying cancer cells *in vitro* relies on 2D monolayer cultures, which in no way represents the physiological tissue microenvironment *in vivo*. Therefore, preclinical and translational cancer research trends move toward organoid studies and 3D biomimetic models to provide more clinical relevance. Here, we set out to generate a bioink consisting of alginate, gelatin, and nanocrystal hydroxyapatite loaded with primary human osteoblasts and MSCs to produce a robust 3D bone-like microenvironment to study human bone metastasis. A hydrogel (3% alginate; 7% gelatin) model for cancer cell migration was modified to incorporate nanocrystal hydroxyapatite, primary human osteoblasts, and primary human bone marrow-derived stromal cells. Primary osteoblasts were isolated from vertebral bodies of organ donors, and bone marrow MSCs were purchased from Rooster Bio. The constructs were cultured over 28 days in a control medium (DMEM) or osteogenic medium (OM) with and without 0.5 mg/mL nano-hydroxyapatite (HA). Live/Dead® assays were performed to quantify viability, fixed frozen sections were stained with Alizarin Red for calcified matrix deposition, and Mayer's Hematoxylin and Eosin (H&E) staining to observe cells nuclei. High osteoblast viability in all conditions was observed after 28 days of culture: 92.5 ± 2.5 % for DMEM/HA-, 85.9 ± 6.2 % for OM/HA-, 91.3 ± 3.18 % for DMEM/HA+ and 88.6 ± 0.38 % for OM/HA+ respectively. MSCs were cultured for 21 days and showed 71.93 ± 4.59 % for DMEM/HA-, 68.56 ± 5.84 % for

OM/HA-, 63.46 ± 4.78 % for DMEM/HA+ and 63.40 ± 1.16 % for OM/HA+. Moreover, cells grown in DMEM without HA had the least amount of mineralized bone matrix. Cells grown in OM/HA^{+} were found to have the most bone mineralized matrix. Our data indicate that the combination of 0.5 mg/mL nano-hydroxyapatite with OM produces a favorable bone-like microenvironment for primary human osteoblasts and MSCs. Our preliminary work with low-cost bioprinting indicates that this bioink is extrudable and will be ideal for screening therapeutics against patient-derived tumor cells. This work will allow a better understanding of interactions between normal osteoblasts, stromal cells, osteocytes, and patient-derived bone metastatic cells while also placing higher clinical relevance on therapeutics screening.

RÉSUMÉ

L'os est un tissu avec des tendances dynamiques constamment en train de se reformer par une balance d'ostéoblastes et d'ostéoclastes. Cependant, lorsque divers cancers envahissent l'os, cette balance de cellules est perturbée, ce qui entraine des modifications souvent irréversibles dans la structure et la fonction osseuses. Nous avons recours à la radiothérapie, la chimiothérapie ainsi qu'à des procédures chirurgicales afin de traiter la métastase des os. En ce moment, étudier les cellules cancéreuses *in vitro* est un processus qui repose sur des cultures 2D, ce qui ne représente, en aucun cas, le milieu 3D retrouvé chez l'humain. Ainsi, les tendances de la recherche préclinique et translationnelle sur le cancer semblent promouvoir l'utilisation de modèles 3D comme les organoïdes afin de fournir plus de pertinence clinique. Ici, nous avons généré une bio-encre composée d'alginate, de gélatine et de nanocristaux d'hydroxyapatite chargée d'ostéoblastes humains primaires et de cellules souches mésenchymateuses dans le but de produire un modèle 3D ressemblant au microenvironnement de l'os humain pour étudier les métastases osseuses humaines. Un modèle à base d'hydrogel (3% alginate; 7% gélatine) utilisé pour évaluer la migration de cellules cancéreuses a été modifié pour incorporer des nanocristaux d'hydroxyapatite, des ostéoblastes primaires et des cellules stromales primaires dérivées de la moelle osseuse humaine. Les ostéoblastes primaires ont été isolés de corps vertébraux appartenant à des donneurs d'organes et les cellules souches ont été achetées par Rooster Bio. Les modèles ont été cultivés pour une durée de 28 jours dans un milieu contrôle (DMEM) ou un milieu ostéogénique (OM) avec et sans 0.5 mg/mL d'hydroxyapatite (HA). Des expériences Live/Dead® ont été effectuées afin de quantifier la viabilité des cellules, des coupes de tissus gelés fixes ont été colorées avec le rouge d'alizarine pour évaluer le dépôt de matrice calcifiée et la coloration à l'hématoxyline et à

éosine de Mayer afin d'observer le noyau des cellules. Une viabilité élevée des ostéoblastes humains dans toutes les conditions a été observée après 28 jours de culture: 92.5 ± 2.5 % pour DMEM/HA-, 85.9 ± 6.2 % pour OM/HA-, 91.3 ± 3.18 % pour DMEM/HA+ et 88.6 ± 0.38 % pour OM/HA+ respectivement. Pour ce qui en est des cellules souches, après 21 jours d'incubation, nous avons observé des taux de viabilité de : 71.93 ± 4.59 % pour DMEM/HA-, 68.56 ± 5.84 % pour OM/HA-, 63.46 ± 4.78 % pour DMEM/HA+ et 63.40 ± 1.16 % pour OM/HA+. De plus, les cellules incubées dans le DMEM sans la présence de HA avaient la moindre quantité de matrices minéralisées osseuses. Les cellules cultivées dans OM/HA^{+} se sont avérées avec le plus de matrices calcifiées. Nos résultats indiquent que la combinaison de 0.5 mg/mL de HA et du milieu OM favorise un milieu ressemblant le plus à l'os humain. Nos expériences préliminaires à bio-impression à faible coût nous indiquent que cette bio-encre sera idéale pour le dépistage de produits thérapeutiques contre des cellules tumorales dérivées de patients. Nos travaux permettront de mieux comprendre les interactions entre les ostéoblastes normaux, les cellules stromales, les ostéocytes et les cellules métastatiques osseuses dérivées de patients, tout en accordant une plus grande pertinence clinique au dépistage thérapeutique.

ACKNOWLEDGMENTS

There are many people to whom I am indebted, and without them, I could not be able to finish this thesis. I would like to start with my supervisor Derek H. Rosenzweig. I am thankful for everything you have done for me and allowed me the honor of being the first student under your direct supervision. You have been nothing but a source of positivity and enlightenment during my master's degree. You have always been there for me, and I will forever be grateful for your patience with me, teaching me everything I needed to know, assisting me during my experiences, and staying up late with me correcting my abstracts. To Elie G. Akoury, I have nothing but great things to say to you. You have been a fantastic person that I am lucky to have met throughout my master's. You have helped me grow and be an incredible mentor and, most importantly, a friend to me. To Pouyan Ahangar, a wonderful person that I shared terrific moments with. We got along very well as soon as I entered the laboratory. You taught me everything you knew, and it has been great to work with you. I will never forget that night where we went to harvest a spine and got hungry in the middle of the procedure and went out to eat at 2:00 AM. Only great memories with you. To Mina Aziz, you are a very knowledgeable person that I am glad I had around me. I learned so much from you and shared unforgettable memories with you during our classes. To Megan E. Cooke, I would like to thank you for being not only a phenomenal scientist but also a very kind person and providing me with your support whenever I had asked for it. To everyone else that I have had the pleasure to share laboratory space or classes with, I wish you all nothing but the best. I have developed many friendships that I will intend to carry on beyond my master's journey. To Sharon Turner, the Experimental Surgery program coordinator, I would like to thank you from the bottom of my heart for everything she has done for me. Thank you for your exceptional

administrative work and, most importantly, your delicious nacho dip. Lastly, I would like to thank my family for their unconditional support and dedicate this work to my grandfather, Antone Nour *Senior*, who passed away last year. Your passing has shattered me, but I am granting your last wish to graduate, and I hope you are looking down at me smiling.

CONTRIBUTIONS OF AUTHORS

This thesis has been done according to the standard format put forth by the Faculty of Graduate and Postdoctoral Studies (GPS) at McGill University. This thesis contains an introductory chapter, a material and methods chapter, a results chapter, a discussion, and an appendix chapter.

Antone Nour performed all cell cultures, media preparations, gel preparations, staining, cryosections, and images. Megan E. Cooke served the nano-hydroxyapatite synthesis. Megan E. Cooke also performed the SEM.

The collection of human spines and cell isolation from the tissue was performed evenly by every laboratory member.

A first draft of the thesis prepared by Antone Nour was revised based on comments and recommendations of Dr. Derek H. Rosenzweig, who has helped with editing the final version of the thesis.

INTRODUCTION

Bone Development and Physiology

Contrary to popular belief, bones are not inert structures. The bone is a very dynamic organ consisting of living tissues that regularly undergo remodeling throughout one's lifetime. The bones are essential for mobility, but they also protect our soft tissues and function from supporting the whole body [1]. It is also where most of our calcium and phosphate are stored, dictating its importance in the maintenance of mineral equilibrium [2]. Four different types of cells can be found in bones [3]. Those cell types are osteoblasts, osteoclasts, osteocytes, and osteoprogenitors. These cells all have different roles in maintaining a healthy environment within the bones.

Osteocytes are the most abundant cells found in bone. They account for over 90% of the bone cells on the bone surfaces or within the matrix [4, 5]. Based on German surgeon Julius Wolff's work in 1982 [6], he hypothesized that their primary role revolves around mechanosensation, where they would be able to sense strains on the bone surface following physiologic loads. As such, many studies have confirmed his hypothesis and showed that osteocytes are responsible for bone adoption in response to mechanical loading [7, 8]. Furthermore, their bone remodeling properties have been demonstrated by expressing factors affecting bone formation, making them also endocrine cells [9].

Osteoprogenitor cells, also known as osteogenic cells, are mesenchymal stem cells in the bone marrow. They play an essential part in bone growth and repair [10]. They are also commonly referred to as pre-osteoblasts because they are precursors to osteoblasts and osteocytes [11].

The osteoblasts are concentrated on the surface of the bones. They are responsible for synthesizing and secreting bone matrix, also called osteoid. They also have a crucial role in regulating bone mineralization by secreting essential enzymes such as alkaline phosphatase and proteins like type 1 collagen and osteopontin needed for that process [12]. It should also be known that the process of forming osteocytes (osteocytogenesis) and osteoclasts (osteoclastogenesis) is coordinated by osteoblasts [13, 14]. Lastly, there are three possible outcomes for an osteoblast; undergoing apoptosis (cell death), becoming an osteocyte, or flatten and turn into a cell to line the bone surface [15].

Lastly, the osteoclasts are large multi-nucleated giant cells that play a crucial role in bone remodeling. They are responsible for resorbing bone by secreting lysosomal proteases, mainly cathepsin K and matrix metalloproteinases [16]. Simply put, the process of remodeling requires osteoclasts to absorb and break down bone, while osteoblasts construct bone. A stable balance of these two cell types is necessary to have a good quality of the bone structure. Osteoclasts are originally hematopoietic and derive from the monocyte-macrophage lineage of cells. Surrounding cells such as stromal cells and osteoblasts secrete macrophage colony-stimulating factor (m-CSF), a cytokine that, in return, transforms the granulocyte-macrophage progenitor cells into osteoclast precursor cells that now have a RANK receptor [17]. Stromal cells and osteoclasts secreting m-CSF also secrete RANKL. This ligand attaches to the RANK receptor found on these osteoclast

precursor cells, which starts a signaling cascade, inducing nearby precursor cells to fuse and form multinucleated cells, ultimately becoming mature osteoclasts.

Bone, like many other organs or tissues, is subject to cancer growths. There are several types of cancers, where some are classified as primary, others as secondary. Osteosarcomas, chondrosarcomas, and Ewing's sarcomas are perfect examples of primary cancers, while secondary metastatic cancers are highly subjected to breast and prostate cancer patients. They both have devastating effects on the skeleton and can therefore be lethal.

Overview of Cancer

Cancer appears when a random cell stops responding to the body's signal on cell division, starts acting independently, and proliferates uncontrollably. It also evades any growth suppression and can sustain itself by angiogenesis. Once this abnormal cell has proliferated enough to create a mass of cells, it is labeled a tumor. If this tumor happens to invade other types of areas in the body, this ultimately makes it an invasive cancer. Tumors can be either malignant or benign. The main differences between those two are their proliferation speed, how easy it is to stabilize them, and the potential to invade other tissues. Generally, benign tumors proliferate slowly compared to malignant tumors, are usually easier to stabilize since they evolve locally, and are not commonly known to metastasize. The consequences of benign tumors are not life-threatening in most cases. In contrast, malignant tumors are known to infiltrate and destroy other tissues, leading to a fatal outcome [18]. Once removed, the benign tumors present no recurrences, although malignant tumors commonly show recurrences.

Next, depending on the type of cell or tissue that started proliferating, the tumor can be classified into one of many groups: carcinomas, myelomas, sarcomas, lymphomas, leukemias, and mixed types. 80 to 90 percent of all cancer cases have been classified as carcinomas [19]. Simply, carcinomas are abnormalities coming from epithelial cells. Epithelial cells cover the ins and outs of the surfaces throughout the human body like organs, for example. Upon being classified as a carcinoma, tumors can then fall into either adenocarcinoma or squamous cell carcinoma subtypes. If the tumor develops in an organ or a gland, it is called adenocarcinoma, and if it arises from the squamous epithelium, it is then labeled as squamous cell carcinoma. Myelomas are cancers that arise from plasma cells of the bone marrow. Sarcomas are solid tumors that originate from connective tissues like the cartilage, bone, and muscle predominately. Lymphomas come from cells of the immune system, while leukemias come from the blood-forming cells. In short, there are hundreds of different types of cancers that all emerge from uncontrolled and abnormal cell proliferation that can originate from any cells in the human body, and each of these types of cancers is unique on its own [20].

Consequently, to achieve staging and classification of a tumor, a protocol is recognized as a world standard by the American Joint Commission on Cancer Staging [21]. It is the TNM classification, devised by the International Union Against Cancer (UICC). This classification is based on assessing the tumor, the regional lymph nodes, and the distant metastasis. The letter T (tumor) represents the size of the primary tumor where T0 implies the absence of tumors while T1, T2, T3, and T4 respectively imply the tumor's maximum diameter size is 2.0 cm or less in the greatest dimension (T1: T < 2 cm), the tumor's full diameter size is more than 2.0 cm, but not more

than 4.0 cm in greatest dimension (T2: 2 cm ≤ T ≤ 4 cm), the tumor's maximum diameter size is more than 4.0 cm in greatest dimension (T3: T > 4 cm), and the tumor's diameter is of any size with direct extension to a chest wall of skin (T4) [22]. Next, the letter N (nodes) represents the regional lymph nodes' involvement, where N0 implies the absence of regional nodal. Meanwhile, N1, N2, and N3 respectively suggest that there is some level of nodal spread; N1 being metastasis in 1 to 3 regional lymph nodes (N1: $1 \leq N \leq 3$), N2 being metastasis in 4 to 6 regional lymph nodes (N2: $4 \leq N \leq 6$) and N3 being the most progressive spread, metastasizing in up to 7 or more regional lymph nodes (N3: $N \geq 7$) [18]. Finally, the letter M (metastasis) represents the presence of distant metastases, where M0 implies the absence of distance metastasis while M1 presupposes the existence of distant metastasis.

After taking the T, N, and M results into account, health care professionals can determine the patient's stage of cancer. There are four different stages where stage IV is the most severe stage.

Starting, stage 0 represents cancer *in situ*, or, in other words, cancer in place, is where no form of spreading to other tissues by the abnormal cells has been observed. The cancer is classified as early-stage and is very treatable by employing radiotherapy or surgery to remove the cells properly. Next, stage I cancer, also early-stage cancer, is where no form of spreading by the tumor has been observed. Along with stage 0 cancer, stage I cancer is highly treatable following immediate treatment such as radiotherapy or surgery. Next, stages II and III can be grouped because they consist of early and late large cancers (T1 to T4). In these stages, spreading to the regional lymph node is generally observed (N0 to N3) but not spread throughout the body (M0). Treatments usually consist of a combination of radiation and chemotherapy. If all fails, surgery

might be an option discussed with the patient. Lastly, stage IV, the most serious one, also known as metastatic cancer, implies that the tumors have spread throughout the body (M1). Therefore, at this stage, chances of survival are significantly lower than in the earlier stages.

According to the public health agency of Canada, in 2019, around 50% of Canadians develop cancer in their lifetime and approximately 25 percent of those that developed it succumb to it. In 2020, 225 800 new cancer cases and 83 300 cancer deaths were expected, according to previously collected data up to 2015 [23]. It was predicted that the most diagnosed cancers would be lungs, breast, and prostate, according to the same data. Respectively, lung, colorectal, pancreatic, and breast cancer were also projected to be the leading causes of death with 25.5%, 11.6%, 6.4%, and 6.1% of mortality. It is also important to point out that the death rate of female breast cancer has dropped by just about 49% since 1986. Together, these four cancers sum up to 49.6% of cancer-related deaths in Canada. Not only are these the most diagnosed and worst death-related cancers, but they are also the most common with bone metastasis.

As for breast cancer, 1 in 8 (13%) females are expected to be diagnosed with breast cancer in their lifetime, making it the most common cancer diagnosis in women. 1 in 33 (3%) females is expected to die. The 5-year net survival (chance of staying alive after the diagnosis) for women with breast cancer in Canada is around 88%. The 5-year relative survival for breast cancer, depending on the stages, goes as follows: 100% for stage 0; 100% for stage I; 93% for stage II; 72% for stage III; 22% for stage IV [24]. Concerning prostate cancer, 1 in 9 males is expected to be diagnosed with prostate cancer in their lifetime, making it the most common cancer diagnosed in males. 1 in 29 (4%) males is expected to die from prostate cancer. The 5-year net survival for

men diagnosed with prostate cancer in Canada is around 93%. The 5-year relative survival for prostate cancer, depending on the stages, goes as the following: 100% for stage 0, I, II, and III; 28% for stage IV (when cancer ultimately spreads to the rest of the body) [24] As for lung cancer, around 1 in 15 Canadians is expected to be diagnosed with lung cancer, and about 1 in 17 Canadians will die from it. The 5-year net survival for women and men diagnosed with lung cancer in Canada is 22% and 15%, respectively. The 5-year relative survival for lung cancer depending on the stages has not been documented for Canada. However, according to what is known, limited-stage SCLC (small cell lung cancer) has a median survival of 12 to 16 months with treatment, and extensive-stage SCLC has a median survival of 7 to 11 months, also with treatment [24].

Bone Metastasis

The process of metastasis occurs when cancer cells split off the primary tumor site and make their way into the lymphatic system or the bloodstream to spread to distant organs and establish new tumor sites, usually referred to as secondary tumors. English surgeon Stephen Paget initially theorized this concept in 1889 where he referred to that process as the ‘’seed and soil’’ theory [25, 26]. Indeed, it was documented that cancer cells undergo a succession of events that will lead them out of the primary tumor site, starting with a loss of cell adhesion and polarization [27], a process now known as epithelial-to-mesenchymal transition (EMT). Next, the secretion of proteolytic enzymes dissipates the extracellular matrix in the surrounding, allowing them to move around and access the stream freely. They will venture to utilize a mechanism called intravasation and ultimately latch on a new position relocate [28, 29]. Then, many events such as proliferation, angiogenesis, and the avoidance of the body’s defense mechanisms occur to ensure the survival

and the growth of the newly located cancer cells [30-32]. From there on, the chances of survival for the patient will be drastically lowered, considering how the principal cause of death in patients who have cancer is from metastasis [33].

Succeeding the liver and the lungs, the third organ most likely to be hindered by the migration of cancer cells from their original site is bone [34]. It is important to emphasize that bone metastasis frequently arises from multiple solid tumors. Even though bone metastasis can emerge from any cancer, it generally originates from organs such as the breast, prostate, and lungs [35-37]. In patients with progressive metastatic disease, the relative incidence of bone metastasis is around 65 to 75% for breast cancer, 65 to 75% for prostate cancer, and about 30 to 40% for lung cancer [38-41]. Unfortunately, these patients have a very low prognosis, and survival rates are restricted to months. Recent studies showed that the 12 months survival for lung, breast, and prostate cancer patients were 10%, 51%, and 35%, respectively. At 60 months, these rates drop to 1%, 13%, and 6%, where it seems that breast cancer patients with bone metastasis undoubtedly have a longer life expectancy [42]. Withal, essential advancements in science and medicine are being made to allow patients with bone metastasis to live as long as possible.

Typically, in patients with bone metastasis, the most common skeletal-related events reported are pain, the presence of multiple fractures, spinal cord compressions, and an overall downturn in regards to the physical condition [43-45]. Many studies have shown that in around 50% of breast cancer patients with bone metastasis, at least one skeletal-related event occurs [46, 47]. The most common sites for bone metastases are the spine, the thoracic cage, the pelvis, and the femurs [48]. Diagnosing bone metastasis can be pretty challenging since it can sometimes

present itself as asymptomatic in some patients. On top of that, more than half of the patients that do have bone metastasis all experience nonspecific pain, making it even harder to associate it with the condition directly. However, bone metastasis can be diagnosed employing CT scans, plain films, biopsies, or even scintigraphy [49]. Moreover, factors such as sensory loss, rest pain, night pain, and overall weakness are signs that could lead to a positive diagnosis of bone metastasis [43].

Spine Metastasis

The majority of patients with metastatic cancer will form secondary tumors in the bone organ. As mentioned, the most common area where these secondary tumors develop is the spine. Spine tumors seem to be more present in the lumbar region, followed by the thoracic and cervical spine areas [50]. Depending on their location on the spine, they are classified as either extradural or intradural spinal tumors. It has been documented that nine patients out of ten will ultimately have extradural spinal metastases [51, 52].

There are many different ways these tumors can appear. Firstly, cancer cells from the primary neoplasm can be carried from the arterial system and delivered to the bone marrow, where they will slowly grow, which, in return, will result in spinal cord compression. This process is known as the most common way to develop metastases in cancer patients. Secondly, cancer cells can technically also be transported via the venous system. Studies have shown that the Batson veins might spread cancer cells from their primary location due to their valveless characteristics, leading to deposition in the epidural space [53]. Metastases that arise from this way come mainly from primary cancers originating from pelvic organs such as the prostate. Another way that

metastatic tumors can rise, a lot rarer, is when tumor cells can be transported by the cerebrospinal fluid (CSF) in patients with glioblastoma and find themselves in a clump of nerves below the extremity of the spinal cord also called ‘’cauda equina’’ [54]. According to a study where authors reviewed and studied 600 cases of spine metastasis, people between the ages of 40 and 70 have the highest incidence of spine metastasis since, at this age, people start developing different underlying conditions, thus, exposing themselves to all sorts of pathologies [55].

Types of Metastatic Lesions

For a normal bone microenvironment to be present, healthy communication between osteoblasts and osteoclasts is required. However, in spine metastases, cancer cells have successfully migrated from their original site to find themselves at the spine and have already disrupted this healthy balance. Consequently, the spine is the most common site where we will find cancer cells that have migrated from their original location, which mainly are: the prostate, the breast, or the lungs [56]. Thenceforth, depending on how the bone components and remodeling are being affected and following x-ray images, spine metastases can be classified as osteolytic, osteoblastic, or even a mixture of both. An osteoblastic lesion, also known as bone remodeling metastasis or bone-forming, is characterized by an increased number of osteoblasts, which usually is related to an increased bone production. On the x-rays, it is manifested by a thick, non-flexible, and rigid bone structure. An osteolytic lesion, also known as a destructive bone metastasis or bone-resorbing, is quite the opposite. It is characterized by an increased number of osteoclasts, usually related to a bone breakdown (or thinning). Instead of noticing an important concentration of bone components on the x-rays, here we see up to 50% of the bone structure destroyed by the tumor

[43]. This destruction (or osteolysis) of the bones leaves visible holes on the x-rays referred to as lucencies.

Consequently, osteoblastic lesions are most likely to emerge from prostate cancer, carcinoid, and small cell lung cancer [57]. Osteolytic lesions usually develop from multiple myeloma, renal cell carcinoma, and thyroid cancer, to name a few [58]. As for patients that present a combination of osteoblastic and osteolytic lesions, the mechanisms are still not fully elucidated and will be needing further research. However, both these lesions can be found in patients affected by squamous cell carcinoma, breast or gastrointestinal cancers.

Treatments

In the past few years, the spine oncology field has been growing quickly, as treating primary bone tumors of the spine is more demanding. In terms of cures, nothing is available at the moment, unfortunately. Once the patient has been diagnosed with spine metastasis, the condition is generally labeled as incurable. Every resource is redirected to treat the symptoms, such as reaching tolerable pain levels and achieving stability of the spine rather than the condition itself [59-61]. Depending on the severity of the symptoms, different options may be offered to the patients, such as radiotherapy, chemotherapy, hormonal therapy, and surgical resection. Technological advancements, especially in radiotherapy, are making an appearance recently, and they seem very promising to restore the average quality of life in patients [62].

Radiotherapy has been shown to provide relief to a significant portion of patients. With recent advancements in the field, radiotherapy has become the first-in-line treatment for spine metastasis unless spinal cord compression or other complications do not allow the treatment to go through [63]. In cases where compressions are present, surgery will be employed to liberate the area if it does not endanger life. Three-dimensional conformal radiation therapy (3-DCRT), intensity-modulated radiotherapy, stereotactic radiosurgery, and stereotactic body radiotherapy (SBRT) are all techniques that are considered once a patient has been diagnosed [64]. Surgical procedures alone have had considerable advancements in the past decade. Still, significant postoperative pain and extended hospital stays remain big concerns that need to be taken into account [65], which is why multimodal treatment strategies (combination of surgical and radiotherapy) are recommended to some patients, depending on their situation, for maximum results. Many studies have shown the benefits of combining treatment approaches to achieve better patient outcomes [66, 67]. In 2005, a group of surgeons carried on a study to assess the effect of surgery and indirectly show combining surgery and radiotherapy in patients with spine metastasis [68]. In that study, two groups underwent radiotherapy and were given ten 3 Gy fractions (totaling 30 Gy). Only one group was assigned surgery pre-radiotherapy treatment. In summary, results showed that, out of 50 patients in the surgery and radiotherapy group, 42 could walk and retain their ability to walk (84%) versus 29 out of 51 (51.57%) in the radiotherapy-only group. In conclusion, they demonstrated the importance of surgery and that combining two treatment options might result, generally, in a superior outcome for patients.

Surgery remains a great option of treatment, particularly by resecting tumors and decompressing the neurovascular and bony environment surrounding them. Also, implanting

biodevices able to release therapeutics and repair bone defects locally is another critical feature of surgery. However, considering how every patient and cancer is different, we cannot immediately implant biodevices. Many patients, once diagnosed, are given the same first-line treatment, to which some might express a completely different response. As personalized therapy is becoming the subject of many discussions, there is a dire need for a model able to screen multitudes of therapeutics and assess which one is more effective for a given patient. A model of such would help in treating patients at a faster and way more effective rate than the traditional methods.

Mechanism of Action of Bony Metastatic Ingrowth

For better and more accurate models for bone metastases to be made, understanding the mechanism of bony metastatic ingrowth is essential. In short, the capability of cells to remain alive and keep growing after migrating from their original location to a secondary tumor location revolves around a theory called ‘’seed and soil’’ proposed in 1889 by English surgeon Stephen Paget [25]. His observations led him to hypothesize that metastatic cells act as ‘’seeds’’. While they are being carried around in circulation, they can only survive and grow if they land on ‘’fertile soil’’, being the microenvironment of an organ. It seems that these ‘’fertile soils’’ are organically different. They each have their particular peptides, hormones, and the general composition of cells, determining which type of metastases could be developed [69, 70]. The data that shows how specific tumor cells tend to metastasize to selected organs directly supports Paget’s theory of ‘’seed and soil’’, which could lead to therapies not only targeting metastatic cancer cells but also factors that support the viability and proliferation of the cells, growth hormones and angiogenic factors [71].

In Vitro Cancer Models

2D vs. 3D

For decades, flat, two-dimensional (2D) *in-vitro* cell cultures have dominated the research field. Basics of cell biology, drug pathways, drug mechanisms of action, and pathophysiology are all mere examples of what 2D cell cultures have helped us further understand. However, several studies have shown how cell bioactivity resulting from 2D cell cultures differs from *in-vivo* outcomes [72, 73]. Not only that, but gene expression, altered response to treatments because of resistance, and poor ECM-cell interactions are better represented in 3D cell cultures and mimic the human microenvironment in a much more accurate way than 2D cultures [74]. It is physically impossible for flat cultures to represent the complexity of 3D structures found in the human body, which is why researchers and pharmaceuticals are pushing towards developing universal 3D cultures for their pre-clinical studies. Spheroids, tumoroids, tumorspheres, and organoids are all models that look promising because they are the closest thing that can mimic the human cancer microenvironment. Properties like proliferation, gene expression, migration, invasion, and survival can all be observed in these models [75, 76].

Simply put, 3D models can be cultured as aggregates, grown on 3D scaffold materials, or can be embedded in gels. Spheroids are known as aggregates, and these models can replicate the key characteristics found in the human body like the internal structure, drug resistance, cell-cell interactions, and gene expression [77]. There are many ways to make these spheroids, but the most prevalent is to use low cell attachment surfaces, typically well-plates, where cells form aggregates

at the bottom of the round plates [78, 79]. Other fabrication methods include the liquid overlay technique [80, 81], the hanging drop technique [82, 83], the microwell hanging drop technique, and spinner flasks. As for tumoroids, similar methods of fabrication are employed. However, the distinction here is that cancer cells are used to form these models. Consequently, once aggregated, their capacity to behave similarly to in vivo tumors increases [84, 85]. As for tumorspheres, they are formed by cell proliferation in conditions where the surface where they grow on has low adherence [86]. These methods all exploit the fact that cells tend to aggregate and form connections by themselves. Organoids are the closest model that we have to *in vivo* tumors [87]. The reason for that is because they are the scaled-down size of organs and *in vivo* tissues, and depending on how we assemble them, they can replicate the structure of specific organs. There are many ways to develop these organoids, such as using embryonic stem cells (ESCs) [88, 89], induced pluripotent stem cells (iPSCs) [89], somatic stem cells, and cancer cells in defined 3D culture systems [87]. Naturally, having a robust model that can replicate the human microenvironment leads to results that can be expected *in vivo*. Consequently, differences have been observed in 3D models compared to 2D models in different diseases such as breast, lung, and prostate cancer, considering one represents the human microenvironment in a much more accurate way. A study published by Sung and al. compared the functional behavior of human mammary fibroblasts (HMFs) cultured in 3D versus 2D models and their effects on the invasion progression of breast cancer cells [90]. One of the several differences observed was that many hormones such as hepatocyte growth factor (HGF), CXCL12, MMP14, COX2 and TGFβ1 are increased in the 3D models, leading to a greater invasive behavior in the breast cancer cells studied. Other researchers were able to notice an increased rate of proliferation in 3D cultures vs 2D, where cells in 3D cultures kept growing for more than 13 days and cells in 2D cultures stopped expanding at day 7

[91]. In regards to the morphology, the same researchers described the 2D cultured cells as sheet-like, trigonal or polygonal, while the 3D cultured cells were shown to be round, shuttle shape-like, and spread-out. Other researchers looked at the effect of substrate elasticity on breast cancer cell lines and observed that in 3D conditions, cells formed fine spheroids, similar to what could be found *in vivo*. However, 2D cultured cells showed a flat shape [92]. Just like in breast cancer, researchers found similar results in prostate and lung cancer. [93]. For instance, prostate cancer cells co-cultured in a three-dimensional setting with cancer-associated fibroblasts were increased in the spheroid compared to fibroblasts, mimicking what is observed *in vivo*. In contrast, the ratio between these two types of cells in a two-dimensional setting does not reflect what can be seen *in vivo* [94]. Overall, all these studies seem to promote that 3D cultures have a different effect on the cells compared to 2D cultures and mimics the reality with better accuracy.

While these particular 3D models might be the closest thing we have to the breast, lung, and prostate *in vivo* environment, they do not necessarily represent the bone environment. Critical features like osteoblasts, osteocytes and vasculature are missing, which is a significant flaw. To reproduce something similar to that, we need to turn to biofabrication therapies.

3D Bioprinting and Bone Tumor Microenvironment

Over the past few years, researchers have worked on developing 3D models for the bone to represent the human bone microenvironment as close as possible. Knowing that the bone is composed of many different cells with their respective conditions to grow and stay alive, it can be hard to reproduce something similar to the human bone microenvironment on a simple petri dish. The importance of having a model that could illustrate how the human bone behaves is colossal. It could be used to study bone physiology and bone diseases. It can also be used as a platform to discover and develop new therapies to treat bone diseases. An up-and-coming method of biofabrication, 3D bioprinting, is being employed at the moment by researchers in the field to create different models able to mimic human bone structures as much as possible. To start building a model representing the human bone microenvironment, proper matrix and bone components must be present. The ability to bear different types of cells, just like the human microenvironment, is also a feature that needs to be fulfilled in such models [95]. Additionally, nearly all 3D models are missing a well-distributed tumor cell composition.

At the moment, hydrogels are being used to a greater extent to simulate the extracellular matrix of solid tumors such as prostate, breast, and lung because of their tissue-like properties [96-98]. Those biopolymer hydrogels most commonly include alginate, agarose, collagen, fibrin, and hyaluronic acid [99]. Amongst these, alginate, a natural polymer extracted from brown algae with a net negative charge, is probably the most significant one when it comes down to 3D printing because of its rigid structure [100]. One of the issues regarding hydrogels is that most of them can not attain the high mechanical properties found in bone. It is worth considering that there are

essential obstacles with current models, like having an oversimplified structure and limited vascularization, which can be mediated thanks to bioprinting.

Consequently, researchers are using polymeric biomaterials such as poly(α-esters), polyurethanes, and poly(propylene fumarate), which have all been shown to be biocompatible and tailorable to model bone [101]. In addition, hydroxyapatite, the predominant mineral found in bone, is added to the mix to improve the mechanical properties (stiffness) and chemical (matrix secretion) of the scaffolds. Models are then tested with purchasable human cells (osteoblasts and osteoclasts) to assess viability and secretion profiles to see if the model is viable for cells to grow and behave as they would in humans. While using available human cell lines to replicate the bone microenvironment might be great, incorporating normal patient osteoblasts and patient-derived cells has not been done yet. This could very well have the potential of replicating the human microenvironment to an even greater extent since the cells used come directly from individuals and are integrated into the bone model within weeks of harvesting, compared to purchasing frozen cells that might behave differently once put in a 3D bone microenvironment.

Alginate's Chemical Structure and Applications

Alginate is a natural, hydrophilic, and negatively charged polysaccharide commonly used in tissue engineering and one of the most predominant biosynthesized materials [102, 103]. Alginate is a polysaccharide made of blocks of 1-4 linked β-d-mannuronic acid (M) and α-L-guluronic acid (G) monomers [104]. Usually, the molecular structure of alginate can take the form of either several successive repetitions of the M residues (-MMM-), the G residues (-GGG-), or alternating between both residues (-GMGM- or -MGMG-) [105]. Varying the chain of the

mentioned monomers will directly consequence the alginate's ability to devise hydrogels [106]. To name a few examples, alginate-based hydrogels have been used for many years in regenerative medicine [107], drug delivery systems [108], and bioprinting [109].

Gelatin's Chemical Structure and Applications

Gelatin is considered a natural and hydrophilic polymer resulting from either the hydrolysis under high temperatures of collagen or the disintegration of collagen [110]. Coming from the denaturation of collagen, the gelatin's properties and chemical structure resemble the one in collagen [111]. Its appeal to researchers comes from being non-toxic, very soluble, biodegradable, biocompatible, and easy to come by [112]. Moreover, it is a reasonable, low cost, and easy to handle starting point. Gelatin-based hydrogels have already been used for ocular tissue engineering [113], drug delivery systems [114], and bioprinting [115].

Alginate/Gelatin Hydrogels

Hydrogels, in general, offer a microenvironment very similar to the *in vivo* bone metastatic microenvironment [116]. Their high tissue water content, affinity to tissues, and ease of handling are what make them stand out from the other alternatives to 3D models. They also offer further advantages such as prolonged culture periods (over four weeks) of more than one cell type and high stability. The model we are proposing in this thesis is a hydrogel consisting of a mixture of 3% alginate and 7% gelatin that has shown to be highly printable and can also demonstrate high cell viability.

Thesis Objectives

To place a higher clinical relevance on effective drug release from new materials and develop a human 3D bone mimetic model to represent the native tumor microenvironment physiologically, the objectives of this study were to:

a) Develop a consistent method to isolate human osteoblasts and characterize the osteoblasts markers
b) Evaluate the cell viability, matrix deposition, and mechanical properties of our hydrogel with and without nano-hydroxyapatite
c) Optimize and test the reproducibility of bioprinting parameters

General Hypothesis

The purpose of this thesis work is to establish a spine metastasis model that can serve not only as a high throughput screening tool for anticancer drugs but also for biomaterials used in bone repair and assess drug delivery. Doing so might better understand the human bone microenvironment as there are no specific niche models representing spine metastasis. As mentioned previously, animal-based models do not accurately reflect how the human microenvironment behaves or responds to therapeutics, which is why the need for a 3D model is crucial. All in all, we hypothesized that a 3% alginate 7% gelatin model would outperform a 1% alginate 7% gelatin model in replicating the native microenvironment observed in human bone and maintaining the native phenotype of cancer cells once added.

MATERIALS AND METHODS

Cells Lines and Isolation of Primary Human Osteoblasts

Primary human bone marrow-derived stromal cells were purchased from Rooster Bio. As for the primary osteoblasts, in short, they were isolated from cadaveric vertebral bodies of organ donors [117]. Our lab collaborates with Transplant Quebec, which permits us to harvest human lumbar spines from consenting organ donors *(McGill Spinal Tissue Biobank (STB / 2019-4896 valid until 2020-04-11).* The harvest itself is coordinated by the orthopedic spine physicians and several fellows, under the supervision of Dr. Jean Ouellet of the Shriner's hospital for Kids in Montreal, QC. The spines are then brought to the Montreal General Hospital, where X-Rays are performed and then stored on the ice at four degrees Celcius up to a maximum of 16 hours, where the isolation of cells and tissues will then occur. Following this process, the spine is brought inside a sterile tissue culture hood and sprayed with 70% ethanol, limiting contamination. The spine is then cleaned by scraping fat, ligaments, muscles, and tendons off it. Next, using a surgical scalpel, the vertebral bodies are separated from the disc tissues. Next, the selected vertebrae are minced into 1 cm x 1 cm sections and are washed with sterile PBS 1x (USA, Sigma—cat D5652). The bone sections are then ready for digestion. They are placed in a solution of 1.5 mg/mL of collagenase (USA, Gibco, Thermofisher— cat 17101-015), and standard RPMI 1640 growth medium (USA, Gibco, Thermofisher—cat 11835-030) supplied with 10% fetal bovine serum (FBS) (USA, Gibco, Thermofisher—cat 12483-020) overnight in a 37°C incubator. The next day, after the process of digestion is completed, the bone pieces are washed with PBS 3 times and plated in T75 flasks, cultured with an RPMI cell culture medium supplied with 10% FBS, 1%

penicillin/streptomycin (PS) (USA, Gibco, Thermofisher—cat 15070-063) at 37°C in a humidified atmosphere of 5% carbon dioxide (CO_2). Once the cells in the flask reach a confluence of 80%, they can be either used or frozen until needed.

Preparation of the A3G7 Gel

0.4 grams of sodium alginate (USA, Sigma—CAS number: 9005-38-3) and 2.8 grams of type B gelatin from bovine skin (USA, Sigma—CAS number: 9000-70-8) were weighted and each transferred to a 5 mL polystyrene round bottom Falcon tube (Canada, Fisher Scientific— cat 14959-1A) to be sterilized via UV exposure for at least 3 hours. Both powders were then dissolved in a sterile beaker with 40 mL of DPBS, no calcium, no magnesium (USA, Thermofisher, Gibco—14190-144) and mixed using a magnetic stirrer on a hotplate for 1 hour at 40°C and 2 hours at room temperature to achieve a homogeneous composite hydrogel. To eliminate the bubbles, the hydrogel was transferred to a centrifuge tube using a spatula or a 60 mL syringe Luer-Lok tip (USA, BD— catalog number: 309653) then centrifuged at 2000 RPMs for 5 minutes. Then, wrap the cap with parafilm and store it at four degrees Celcius until needed.

Preparation of Osteogenic Medium

The preparation of the osteogenic medium started by weighting 2.08 grams of β-Glycerophosphate disodium salt hydrate (USA, Sigma—CAS number: 154804-51-0) and mixed well with 9 mL of serum-free DMEM medium. Next, the solution was filtered with a 0.2 μm pore filter. Next, a beaker was taken, and the following were mixed:

- 50 mL of DMEM with serum and PS;
- 20 μL of 25 μM dexamethasone (USA, Sigma—cat: D4902-25MG);
- 50 μL of 50 μg/mL ascorbic acid (USA, Sigma—cat: A92902-25G);
- 500 μL of the β-Glycerophosphate solution that was previously done.

Preparation of the 3D Model

A previously reported 3D hydrogel A1G7 (1% alginate; 7% gelatin) model for cancer cell-migration [118] was modified in order to incorporate nano-crystal hydroxyapatite (0.5 mg/mL), primary human osteoblasts (1 x 10^6 cells/mL) and primary human bone marrow derived stromal cells (2 x 10^6 cells/mL) for it to become bone-like.

Once the osteoblasts in culture reached a confluence of at least 80%, trypsinization was employed. Cells were counted, and 1 x 10^6 cells were mixed per mL of the A3G7 gel. Gels were then either hand-casted or printed using a low-cost 3D bioprinter.

Hand-casted gels: 1 mL of the solution of cells + A3G7 gel (1 x 10^6 cells/mL) was put on a six well-plate using a 1 mL pipette, followed by submerging the gel with a solution of Ca^{2+} for less than 5 minutes to crosslink the gels. Once crosslinking was done, the gels were separated into four different media: DMEM with HA, DMEM without HA, osteogenic medium without HA, and osteogenic medium with HA and left in the incubator at 37°C and the media was changed every three days for 28 days.

Printed gels: The solution of cells + A3G7 gel was loaded onto a syringe, attached to a Tissue Scribe 3D bioprinter (Aniwaa, United States). Using the SketchUp software (Trimble, Brossard, QC, Canada), models of 0.6 mm height and 5 mm radius with a pore in the middle to allow future cancer cells to be placed were developed and saved as an STL file for 3D printing. Next, the models were sliced into G-code using Simplify3D software (Simplify 3D, Cincinnati, OH, USA). Gels were printed at 25°C and crosslinked with Ca^{2+}. Once crosslinking was done, the gels were separated into four different media: DMEM with HA, DMEM without HA, osteogenic medium without HA, and osteogenic medium with HA and left in the incubator at 37°C and the media was changed every three days for 28 days.

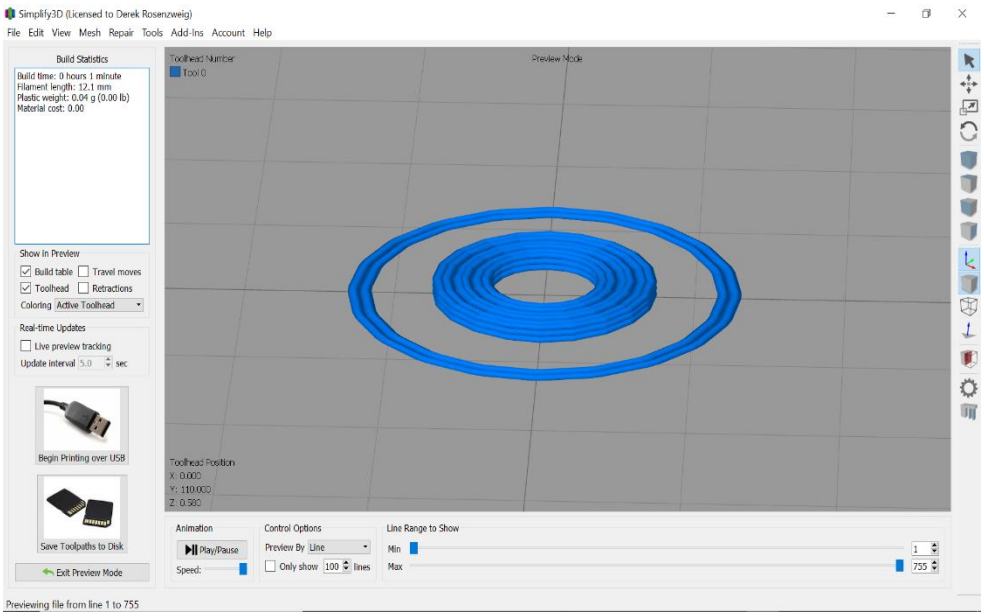

Figure 1: Model being sliced into G-code using Simplify3D software

Considering the height being 0.6 mm and the radius being 5 mm, we can calculate the volume, which adds up to around 50 mm^3 or 0.05 mL. Knowing that the concentration of these constructs is 1 x 10^6 cells/mL, we can safely assume we have about 50 000 cells per construct.

Live/Dead® Viability/Cytotoxicity Assay

The Live/Dead® (LD) assay was performed to quantify the cells' viability in the printed gels after 21 days of culture for MSCs or 28 days for osteoblasts. As such, the LD assay was prepared in serum-free DMEM following the manufacturer's instructions. The LD solution was then placed on each of the gels for 20 minutes. After 20 minutes, pictures were taken using an Olympus IX81 inverted fluorescence microscope from three different positions for each gel. A count for the green cells (alive) and red cells (dead) was done to assess our models' viability. The images were taken using 10x and 4x objectives with MAG Biosystems Software 7.5 (Photometrics, Tucson, AZ, USA).

Cryosection

3D model samples were covered with optimal cutting temperature (OCT) compound (Canada, Thermofisher—23-730-571) and were flash-frozen in liquid nitrogen and stored at −80°C until needed. Once needed, the samples were cut into 12 mm sections using the Leica CM1950 Cryostat (Leica Biosystems Inc., Canada) and transferred onto Fisherbrand™ Superfrost™ Plus Microscope Slides (Canada, Fisher Scientific— cat 22-037-246) and stored in −20°C until needed. Next, samples were dried on a 50°C heat plate for 20 minutes, followed by removing the OCT by

washing in PBS for 5 minutes. The samples were then stained with Alizarin Red and Mayer's Hematoxylin (USA, Sigma—cat MHS32) and Eosin Y (USA, Sigma—cat HT110116-500ML) solutions.

Alizarin Red Solution Preparation

In a beaker, mix 2 grams of Alizarin Red S (USA, Sigma— CAS number: 130-22-3) with 100 mL of distilled water. Mix well and adjust the pH to 4.1 – 4.3 with a 10% ammonium hydroxide solution (Canada, Fisher Scientific— CAS number: 1336-21-6). The Alizarin Red solution, once prepared, will be used to stain our samples and help us identify bone matrix formation by the osteoblasts. Indeed, when the Alizarin Red comes in contact with the bone matrix, it precipitates, and a red coloration can be seen on the samples after being imaged; the redder we see, the more matrix there is.

Alizarin Red Staining

As mentioned previously, Alizarin Red staining is performed to identify bone matrix formation by the osteoblasts in our 3D model. After cryosectioning our samples, the slides are taken and put on a heater for 30 minutes at 50-55°C. Any excess OCT should be removed around the pellet after that. The slides are then dipped into PBS x1 for 5 minutes. Next, the PBS is removed, and the slides are submerged in the Alizarin Red solution and left for around three to five minutes. The slides are then removed and dipped in and out of distilled water and left to dry.

Lastly, the slides are mounted with permount (Canada, Fisher Scientific— CAS number: SP15100), covered with coverslips, and left to dry at room temperature until imaging is done.

Mayer's Hematoxylin and Eosin (HE) Staining

Mayer's Hematoxylin and Eosin staining was performed to differentiate the nuclei from nano-hydroxyapatite particles within our model. After methanol (Canada, VWR—BDH1135-4LP) fixation of the slides (stored at -20°C), the slides are dipped in Milli-Q water and immediately removed from the water three times. Next, we dipped the slides in a prepared 1:1 ratio of Milli-Q water and hematoxylin solution for two minutes. After that, the slides are put under running tap water for 5 minutes. The slides are then dipped in and out of Milli-Q water immediately 20 times. Following that, slides are immersed in 95% ethanol (USA, Thermofisher— cat HC1001GL). Then, the slides are dipped in eosin for 1 minute. Next, the slides are immersed in 70% ethanol and immediately removed 20 times. Afterward, the same is done, but this time with 95% ethanol. After this, the slides are dipped in 100% ethanol for 10 minutes. Then, inside the fume hood, the slides are immersed in xylene (Canada, Fisher Scientific— CAS number: 1330-20-7) for 10 minutes. Lastly, the slides are mounted with permount and covered with coverslips and left to dry at room temperature until imagery is done.

Scanning Electron Microscopy (SEM)

The acellular construct samples were first dehydrated with five different concentrations of ethanol (70%, 80%, 90%, 95%, and 100%), followed by hexamethyldisilazane (HDMS, Sigma Aldrich, Oakville, ON) to dry overnight.

The samples with cells seeded were fixed with a solution of 4% paraformaldehyde (PFA, Sigma Aldrich) for one hour before being dehydrated with five different concentrations of ethanol (70%, 80%, 90%, 95%, and 100%) and hexamethyldisilazane.

With an ACE600 High Vacuum Sputter Coater (Leica Microsystems), all samples were coated with a 4 nm layer of platinum before imaging. Images were taken using an FEI Quanta 450 ESEM (Thermofisher, Saint-Laurent, QC)

Nano-Hydroxyapatite Synthesis

The nanocrystalline hydroxyapatite (nanoHAp) was prepared following the precipitation method published by Mobasherpour et al. [119]. Using a 28-30% ammonia solution (USA, Sigma— cat: 105423), we adjusted the pH to 10 of a 350 mL solution of 290 nM calcium nitrate tetrahydrate (USA, Sigma— cat: C1396). Next, a 250 mL solution of 240 nM ammonium phosphate dibasic solution (USA, Sigma— cat: 70705) was added to the previous solution using a burette while maintaining the pH between 9-11, utilizing the 28-30% ammonia solution previously mentioned. After adding all the ammonium phosphate dibasic solution, the final

solution was left stirring overnight. The next day, the solution was centrifuged at 2000g for 5 minutes. After that, the supernatant was entirely removed. The precipitate was washed with distilled water and centrifuged four more times to remove any residual ammonium that could still be present. After drying the solution using an oven at 65°C for 6 hours, we were left with 12% w/v mineral content.

Protein Extraction by 4M Guanidine Hydrochloride

After 28 days of culture, our 3D model samples are put in a 2 mL tube, and 500 µL of a solution of 4M guanidine hydrochloride is added to break off the membrane of the cells and release the proteins. The tubes are then taken to a four degrees Celcius room and placed onto a rotating shaker for 48 hours to allow the guanidine enough time to dissolve the entirety of the gel. After that, the tubes are centrifuged at 13 000 RPM to remove the non-soluble proteins. We collect the supernatant, transfer it to a new 2 mL tube, and store it at -20°C until needed.

Preparation of Western Blot Samples from 3D Printed Gels

The preparation of WB samples from 3D printed gels starts by thawing the aliquots and transferring 100 µL into new tubes. Next, cold 100% ethanol is added until the final volume of the tube is 1 mL and stored at four degrees Celcius overnight or -20°C for at least 2 hours. Next, to precipitate the soluble proteins, the tubes are centrifuged at 13 000 RPM for 30 minutes at four degrees Celcius. The supernatant is then removed, and cold 90% ethanol is added until the final volume of the tube is 1 mL. The tube is then vortexed to dismantle the proteins. The tube is then

centrifuged at the same conditions again. After the centrifugation, the supernatant is removed, and the tubes are inverted and left to dry for at least 30 minutes until the ethanol has completely evaporated. Lastly, the proteins are suspended with 50 μL of loading buffer until the western blot setup has been done.

Western Blot

In brief, western blotting is a process used in biology to identify specific proteins in a sample. After extracting the proteins from our models and isolating them, they can be detected using the western blot technique.

Running phase

12-well Novex™ WedgeWell™ 4-20% gradient precast gels (USA, Thermofisher— cat: XP04202BOX) are used to assess the identification of osteopontin, collagen I, and sclerostin in our models. Every well is loaded with 15 μL of protein samples from each of our four different model conditions (cultured with DMEM in the presence or not of nano-hydroxyapatite and cultured in osteogenic media in the presence or not of nano-hydroxyapatite). To estimate the molecular weight (MW) of the different sample sizes, 8 μL of a protein standard was loaded into the gel (USA, Thermofisher— cat: LC5925). Our controls, guanidine, went through the same preparation process as our other samples and were used as a positive control, with 10 μL loaded. As for our negative control, acellular gels were used, as they have no protein content in them, guaranteeing no bands visible upon completing the blot. As for our loading control, beta-actin was

used. The gels usually run for around 45 minutes to an hour at 25 mA/gel in standard 1x Tris-Glycine SDS running buffer. The purpose of this step is to transfer the proteins from the wells to the gel itself.

Transfer phase

Next, once the samples have reached the bottom of the gel (indicated by the protein standard), the running phase is over, and we move on to the transfer phase. This phase aims to transfer the proteins found in the gel on a suitable membrane for antibody staining and detection. This process is done by passing a current all over the gel to the chosen membrane. To do so, a particular setup is required. Often named the ‘’transfer sandwich’’, this setup consists of positively charged end to negatively charged end, one piece of sponge, one piece of Whatman 3MM CHR Sheet (USA, Tisch Scientific— product code: 3030-221) followed by the chosen membrane. In our case, it was the Amersham™ Protran®0.2 µm Nitrocellulose Blotting Membrane (USA, Sigma— cat: GE10600001). Next, we put the gel with the ladder positioned on the left, followed by another piece of Whatman 3MM CHR Sheet, and finish it off with two pieces of sponge. Once the setup is complete, the transfer phase can begin. The sandwich is placed into the blotter and then submerged with transfer buffer. The blotter is then left overnight at four degrees Celcius at 30 mA.

Confirming the Transfer

The next day, the ‘’transfer sandwich’’ is removed from the blotter, and the membrane is placed in a square petri dish where Ponceau S solution (USA, Sigma— CAS number: 6226-79-5) is poured on it and left for approximately a minute. The purpose of the Ponceau S solution is to confirm that the proteins have successfully relocated from the gel onto the membrane in the transfer process done the day before. Once a minute has gone by, the Ponceau S solution is removed, and confirmation of the transfer can then be done. Once the success of the transfer has been established, the membrane is washed by covering it with Tris-buffered saline, 0.1% Tween 20 (TBST), and placing on a rotating shaker for five minutes. Once the five minutes are up, pour out the liquid and rinse the membrane once again with some TBST.

Antibody Staining

After the Ponceau S solution has been thoroughly rinsed off, the membrane is blocked for 45 minutes at room temperature using a 3% bovine serum albumin (BSA) in TBST solution. After 45 minutes, the blocking solution is poured out, and the primary antibodies are added. For the osteopontin (USA, Abcam— cat: ab8448), collagen I (USA, Abcam— cat: ab34710), and sclerostin (USA, Abcam— cat: ab85799), each of these antibodies were added in 1:1000 dilutions in TBST and left for an hour and a half. After the first incubation period, the membrane is washed three times with TBST on the rotating shaker, each wash lasting 10 minutes. Next, depending on which primary antibodies we are staining for, the membrane is stained with either donkey anti-goat or donkey anti-rabbit secondary antibodies conjugated to horseradish peroxidase (HRP) in

1:5000 dilutions in TBST for an hour and a half. After the second incubation period was done, the membrane was washed off three times with TBST for five minutes. When the washing was completed, images of the membrane were taken with the ImageQuant™ LAS 4000 (USA, Cytiva— product number: 28955810) using MBI evolution Borealis plus, a western blot detection solution (Canada, Montreal Biotech Inc., product number: BORA-200ML).

Buffer recipes

Tris-Glycine SDS Running Buffer 10X

In a 1L beaker, mix 800 mL of Milli-Q water with 30.2 grams of TRIS base or Trizma® (USA, Sigma—cat: T1503), 144.2 grams of glycine (USA, Sigma—cat: G8898), and 10 grams of SDS (USA, Sigma—cat: L3771). Once the ingredients have dissolved, transfer everything to a clean 1L glass bottle and measure the pH. Once measured, the pH should be around 8.3-8.6. When needed for western blotting, this stock solution should be diluted from 10X to 1X.

Transfer Buffer

In a 1L beaker, mix 700 mL of Milli-Q water with 200 mL of methanol and 100 mL of the 10X Tris-Glycine SDS running buffer. Transfer everything to a clean 1L glass bottle.

Tris-Buffered Saline 10x (TBS)

In a 1L beaker, mix 900 mL of Milli-Q water with 24 grams of TRIS base and 88 grams of NaCl and keep stirring until everything is dissolved. Adjust the pH to 7.6 and the final volume to 1L. When needed for western blotting, this stock solution should be diluted from 10X to 1X.

Tris-Buffered Saline, 0.1% Tween 20 (TBST)

In a 1L beaker, mix 900 mL of Milli-Q water with 100 mL of 10X TBS and 1 mL of Tween 20 (USA, Sigma—cat: P1379)

Loading Buffer

In a 1 mL tube, mix 70% Milli-Q water with 25% of 4x LDS (USA, Thermofisher— cat: NP0007) and 5% 2-Mercaptoethanol (USA, Sigma— CAS number: 60-24-2). The tube is then put at 85°C for 10 minutes before usage.

Densitometry using ImageJ

Using ImageJ, it is possible to compare the density of different bands on a western blot, referred to as densitometry. Quantifying the number of pixels found on the various bands gives us an idea of the protein content.

The first step to densitometry using ImageJ is to convert the picture to 8-bit, found under *Image > Type > 8-Bit.*

Next, using the rectangle selection tool found on the ImageJ toolbar, we highlight the area of interest, in our case, a singular western blot band.

After highlighting the area of interest, we fix the rectangle size by going to *Analyze > Gels > Select First Lane.*

Then, the fixed rectangle can be dragged onto the other areas of interest, and once the rectangle is in place and ready to be set, we go to *Analyze > Gels > Select Next Lane*.

Once the fixed rectangle selection makes it to the last area of interest, we go to *Analyze > Gels > Plot Lanes.*

At this point, a window with profile plots will appear for each of the bands selected with the rectangle tool earlier.

Most of the plots drawn will come with a background signal, and to eliminate that background signal, the Straight-line selection tool is used, and a line is drawn from the beginning of the slope to the end of it. This is what it should look like:

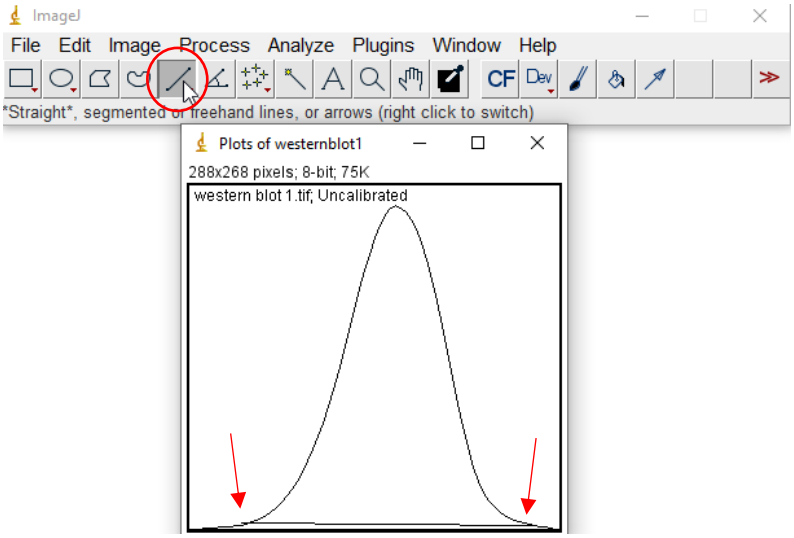

Once the line has been drawn, we will use the Wand (tracing) tool found on the toolbar and click inside the peak. This will, in return, result in a measurement known as the ‘’Area’’ or ‘’Pixel Density’’ for this context.

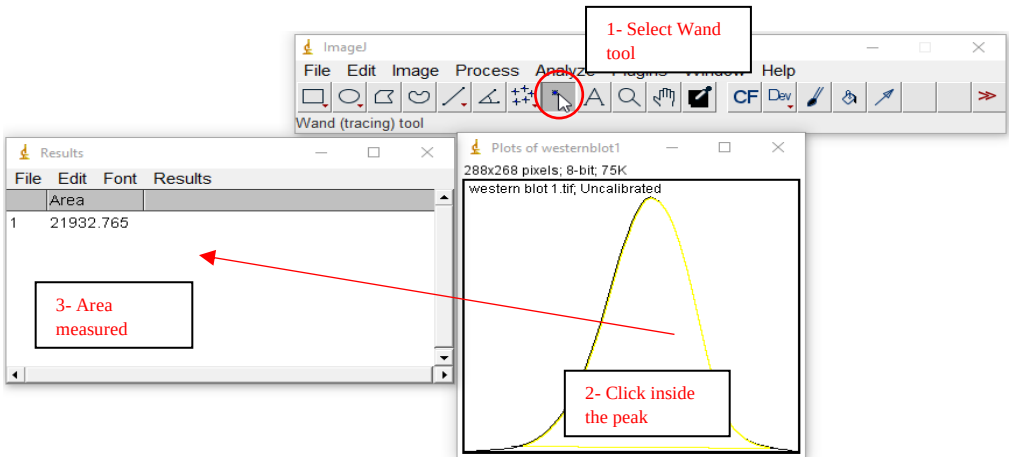

Preliminary Migration Assay

Regular constructs using osteoblasts were labeled using Vybrant Dil Cell-Labeling Solution (Thermo—cat #V22885), and Green Fluorescent Protein (GFP) tagged MDA-MB-231 breast cancer cells were incorporated. The co-culture interaction was observed for five days with daily media change. Pictures were taken using an Olympus IX81 inverted fluorescence microscope. This assay was done once (n = 1) and served as a proof of concept.

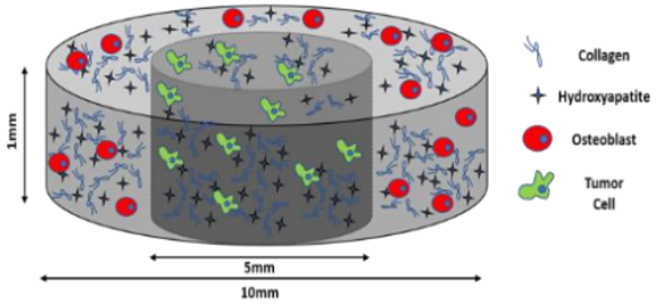

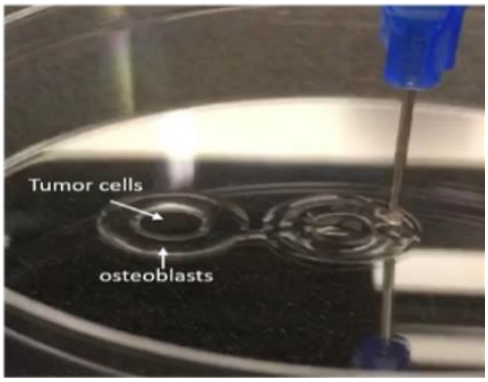

RESULTS

Upon hand-casting and 3D printing our models, the next step was to assess their viability, the matrix deposition, the bone-specific markers, and mechanical properties. The first section of the results will be centered on the hand-casted gels as this was the first step to ensure that the model was functional and count as a proof of concept to move on to the three-dimensional bio-printing process confidently.

Cell Viability (Hand-Casted Models with Osteoblasts)

First, to assess the viability, the Live/Dead® assay was performed. After 28 days of culture, the data shows that human osteoblasts from three different donors were viable within four different media compositions.

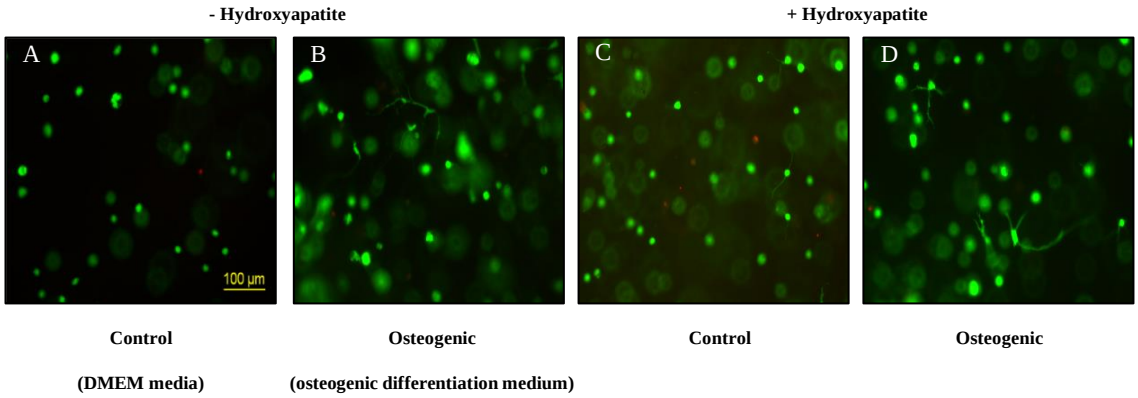

Figure 2. Viability assay. The experiment was done on three different primary cells from donors in four different conditions each; A, control medium (DMEM); B, osteogenic medium (OM); C, control medium + hydroxyapatite (HA+, DMEM) and lastly D, osteogenic medium + hydroxyapatite (HA+, OM). Pictures were taken using an Olympus IX81 inverted fluorescence microscope after 28 days of culture.

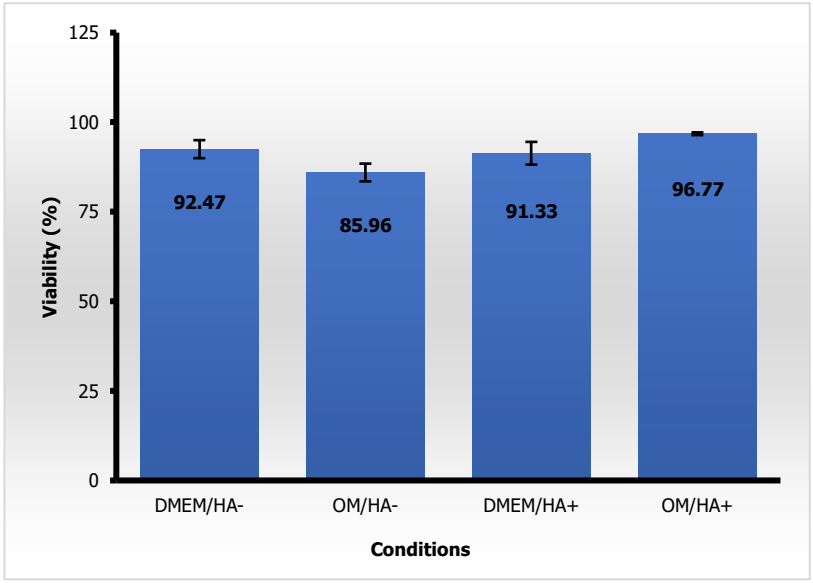

Figure 3. Viability assay. This histogram represents the viable cells in every condition of the experiment after 28 days of culture in form of percentage. The results show a viability of 92.47 ± 2.51 % for DMEM/HA-, 85.94 ± 6.17 % for OM/HA-, 91.33 ± 3.18 % for DMEM/HA+ and 88.59 ± 0.38 % for OM/HA+ respectively.

Indeed, the Live/Dead® analysis revealed strong primary human osteoblast viability in all conditions after 28 days of culture: 92.5 ± 2.5 % for DMEM/HA-, 85.9 ± 6.2 % for OM/HA-, 91.3 ± 3.18 % for DMEM/HA+ and 88.6 ± 0.38 % for OM/HA+ respectively.

Matrix Deposition (Hand-Casted Models with Osteoblasts)

Alizarin Red staining was performed on the samples to reveal the presence of a calcified bone matrix. When the Alizarin Red comes in contact with the calcified bone matrix, the solution precipitates and makes a red coloration visible.

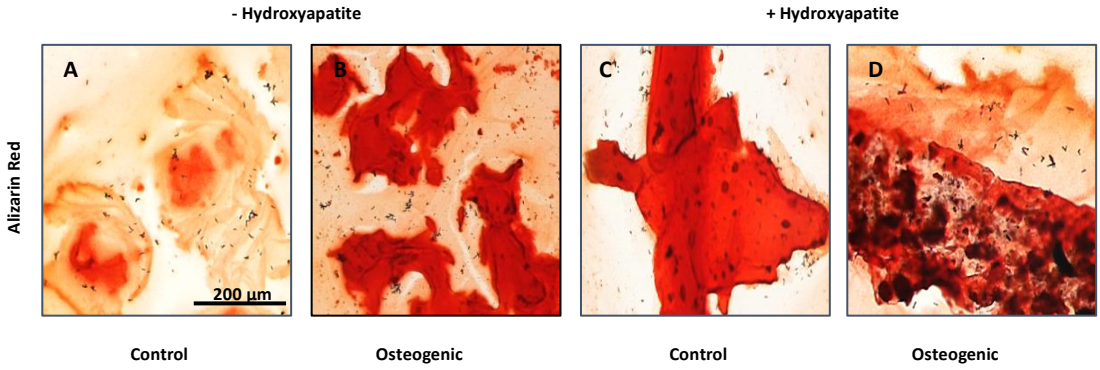

Figure 4. Alizarin Red staining. This figure represents the presence of calcified matrix within four different media conditions after 28 days of culture. The media used were A, control medium (DMEM); B, osteogenic medium (OM); C, control medium + hydroxyapatite (HA+, DMEM) and lastly D, osteogenic medium + hydroxyapatite (HA+, OM). Pictures were taken using an Olympus IX81 inverted fluorescence microscope.

It is important to note that these results represent three independent experiments (n = 3). At first glance, figure 4 shows a striking difference between both the control models and the osteogenic models without hydroxyapatite, which leads us to believe, from our experiment, that the osteogenic media alone can promote the secretion of the bone matrix after 28 days of culture. The same observation can be assessed upon comparing both control models with and without hydroxyapatite and deduct that the secretion of the bone matrix can be influenced by the hydroxyapatite alone. It also seems that combining both hydroxyapatite and osteogenic media promotes a more calcified matrix.

Next, Mayer's Hematoxylin and Eosin (HE) staining was employed to reveal a wide-ranging amount of information on the cytoplasmic, extracellular matrix, and nuclear features that would ultimately help distinguish between the nano-particles of hydroxyapatite and the osteoblast nuclei found in our model.

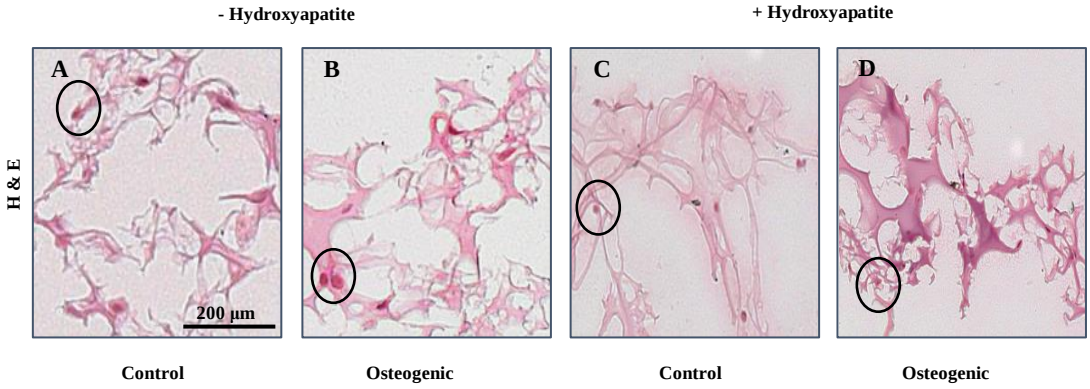

Figure 5. Mayer's Hematoxylin and Eosin (HE) staining. This simple assay shows the presence of nuclei in our model. The circles indicate an example of what the nuclei look like once the staining done. The black dots are representative of the particles of hydroxyapatite. A, control medium (DMEM); B, osteogenic medium (OM); C, control medium + hydroxyapatite (HA+, DMEM) and lastly D, osteogenic medium + hydroxyapatite (HA+, OM)

Cell Viability (3D Bioprinted Models with Osteoblasts)

The same experiments were held out once again, but this time, the models were 3D printed. It is essential to understand that cells go through much stress during bioprinting, such as getting squeezed through narrow needles, being under pressure while the printing process is occurring, and being directly affected by sheer force. The bioprinted models impose a huge challenge considering that the extruding force from the bioprinter has a significant effect on the viability of the cells and could theoretically have a completely different outcome, as shown with the hand-casted gels.

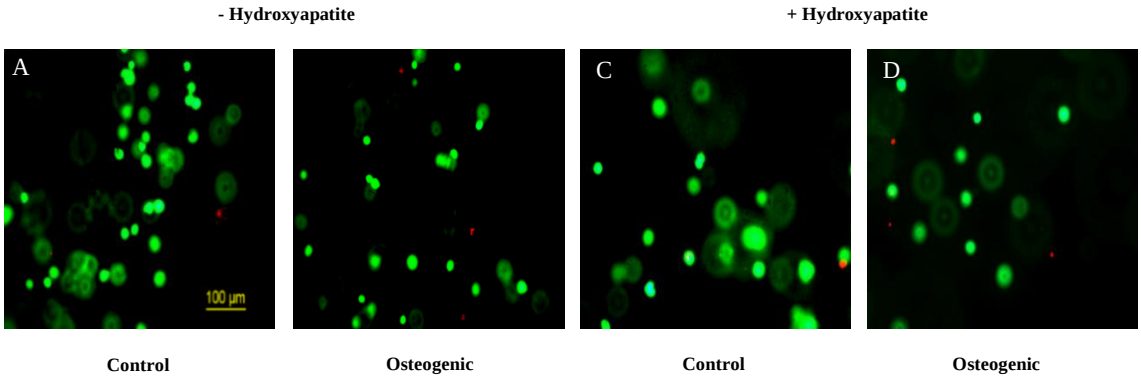

Figure 6. Viability assay. The experiment was done on three different primary cells from donors in four different conditions each; A, control medium (DMEM); B, osteogenic medium (OM); C, control medium + hydroxyapatite (HA+, DMEM) and lastly D, osteogenic medium + hydroxyapatite (HA+, OM). Pictures were taken using an Olympus IX81 inverted fluorescence microscope after 28 days of culture.

Live/Dead® analysis of the newly 3D bioprinted models shows that the cells are indeed viable after going through the extrusion process. The overall viability seems to be comparable to the hand-casted gels. The results show a viability of 87.71 ± 4.36 % for DMEM/HA-, 87.30 ± 4.93 % for OM/HA-, 88.43 ± 1.55 % for DMEM/HA+ and 84.16 ± 3.13 % for OM/HA+ respectively. It seems like the extruding force did not have a significant effect on the viability as we thought it might have.

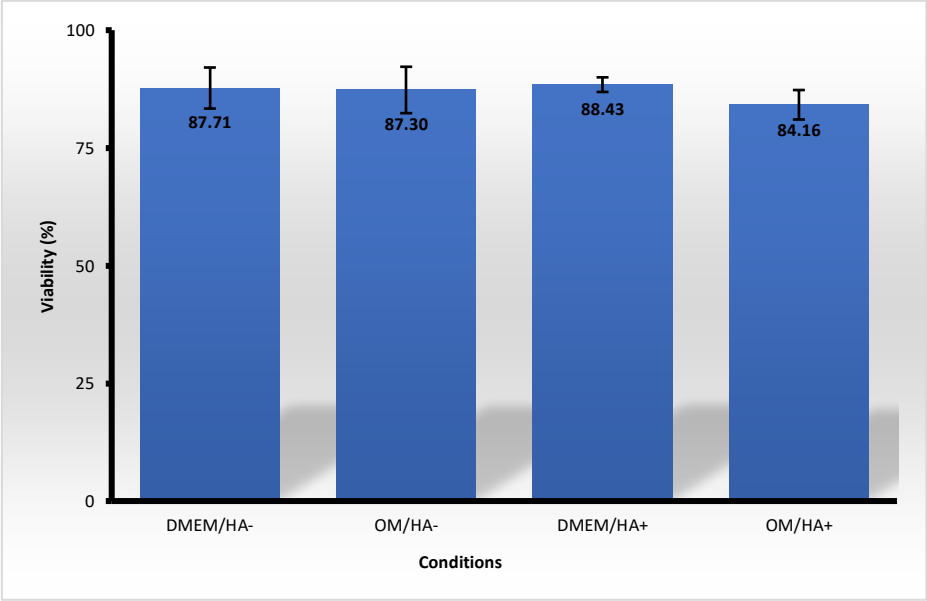

Figure 7. Viability assay. This histogram represents the viable cells in every condition of the experiment after 28 days of culture in form of percentage. The results show a viability of 87.71 ± 4.36 % for DMEM/HA-, 87.30 ± 4.93 % for OM/HA-, 88.43 ± 1.5

Matrix Deposition (3D Bioprinted Models with Osteoblasts)

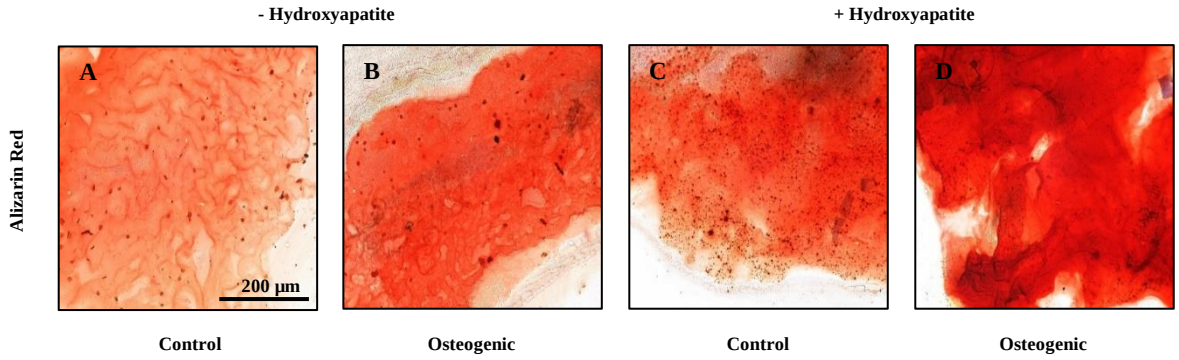

Figure 8. Alizarin Red staining. This figure represents the presence of calcified matrix within four different media conditions after 28 days of culture. The media used were A, control medium (DMEM); B, osteogenic medium (OM); C, control medium + hydroxyapatite (HA+, DMEM) and lastly D, osteogenic medium + hydroxyapatite (HA+, OM). Pictures were taken using an Olympus IX81 inverted fluorescence microscope.

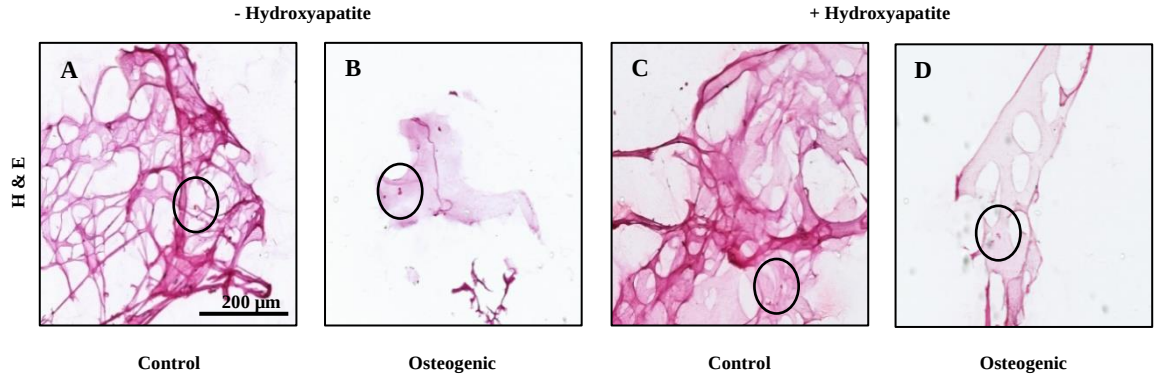

Figure 9. Mayer's Hematoxylin and Eosin (HE) staining. This simple assay shows the presence of nuclei in our model despite the presence of nano-particles of hydroxyapatite that could be hard to distinguish from. The circles indicate an example of what the nuclei look like once the staining done. A, control medium (DMEM); B, osteogenic medium (OM); C, control medium + hydroxyapatite (HA+, DMEM) and lastly D, osteogenic medium + hydroxyapatite (HA+, OM)

Figures 8 and 9 show the same characteristics as Figures 4 and 5. Both sets of figures demonstrate the impact on bone matrix production of both the osteogenic medium and hydroxyapatite alone. Similarly, combining both seems to amplify the production of that matrix. Overall, there are no differences noticed between the hand-casted models and the bioprinted ones.

Cell Viability (3D Bioprinted Models with hMSCs)

After conducting the 3D bioprinting of the models with osteoblasts, new models were bioprinted but with human mesenchymal stem cells (hMSCs) instead. In general, osteoblasts are hard to come by, as they are not available to everyone. On the other hand, hMSCs can be purchased and differentiated into osteoblasts, making them a great alternative model. The interest in bioprinting hMSCs in our model was to ultimately assess if, under specific cell media (osteogenic media), the hMSCs would successfully differentiate into osteoblasts and be used as an alternative model. The results show viability of 71.93 ± 4.59 % for DMEM/HA-, 68.56 ± 5.84 % for OM/HA-, 63.46 ± 4.78 % for DMEM/HA+ and 63.40 ± 1.16 % for OM/HA+ respectively. Based on our results, we can conclude that hMSCs seem more sensitive than osteoblasts (fig. 10 and 11).

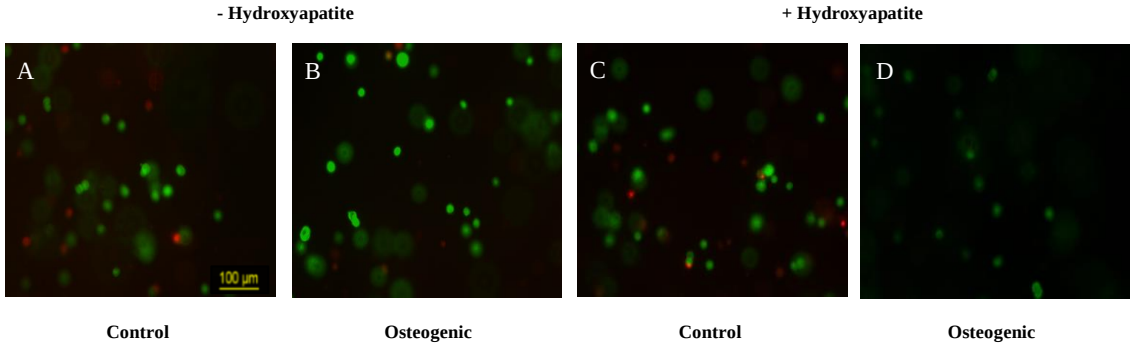

Figure 10. Viability assay. The experiment was done on three different primary cells from donors in four different conditions each; A, control medium (DMEM); B, osteogenic medium (OM); C, control medium + hydroxyapatite (HA+, DMEM) and lastly D, osteogenic medium + hydroxyapatite (HA+, OM). Pictures were taken using an Olympus IX81 inverted fluorescence microscope after 21 days of culture.

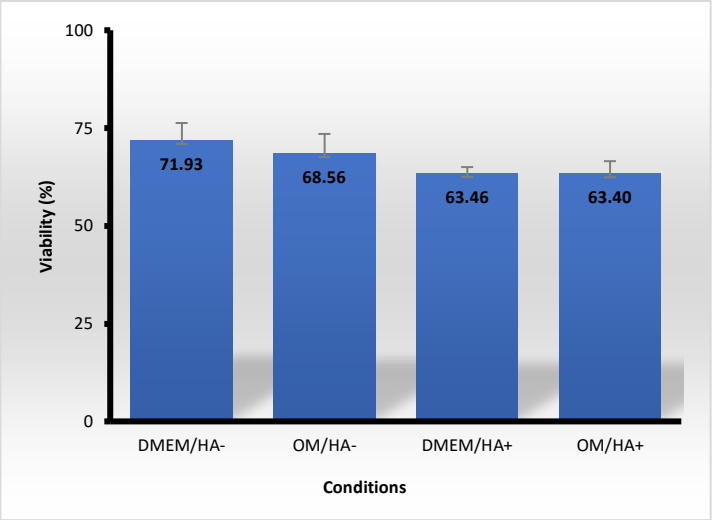

Figure 11. Viability assay. This histogram represents the viable cells in every condition of the experiment after 28 days of culture in form of percentage. The results show a viability of 71.93 ± 4.59 % for DMEM/HA-, 68.56 ± 5.84 % for OM/HA-, 63.46 ± 4.78 % for DMEM/HA+ and 63.40 ± 1.16 % for OM/HA+ respectively.

Matrix Deposition (3D Bioprinted Models with hMSCs)

As a proof of concept, it is vital to assess if, after being conditioned in osteogenic media for 21 days, the hMSCs would differentiate into osteoblast and start secreting bone matrix. A successful differentiation can be observed with a simple Alizarin Red assay, as previously shown. Consequently, for this experiment, we took constructs that had hydroxyapatite present and placed them in either DMEM or OM. After 21 days, Alizarin Red staining was performed.

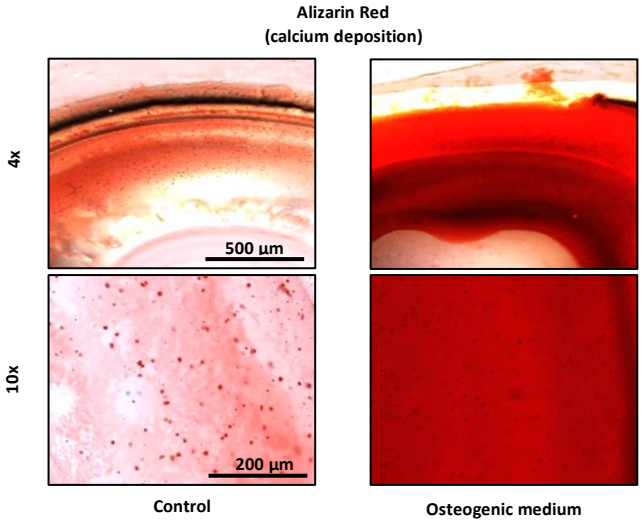

Figure 12. Alizarin Red staining. This figure represents the successful differentiation of hMSCs in our models based off the different levels of calcified matrix secreted. The two similar constructs conditioned in control medium (DMEM) and osteogenic medium for 21 days. Pictures were taken using an Olympus IX81 inverted fluorescence microscope.

Western Blot Analysis

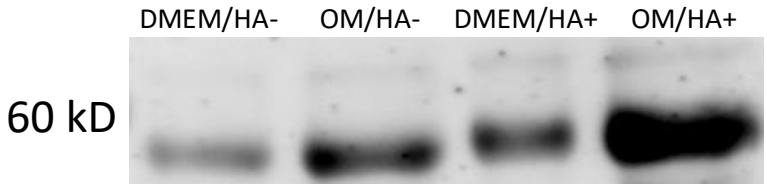

Figure 13: Representative image of the Western blots performed

From three different experimental replicates (n = 3), we were able to quantify, using densitometry via ImageJ, the content of osteopontin found in our constructs normalized to 50 000 cells. Detecting the osteopontin is very important as it is one of the predominant components of the bone matrix. This gives us a clear idea of how the nano-hydroxyapatite and the osteogenic media affect our cells' activity to produce this bone component [120].

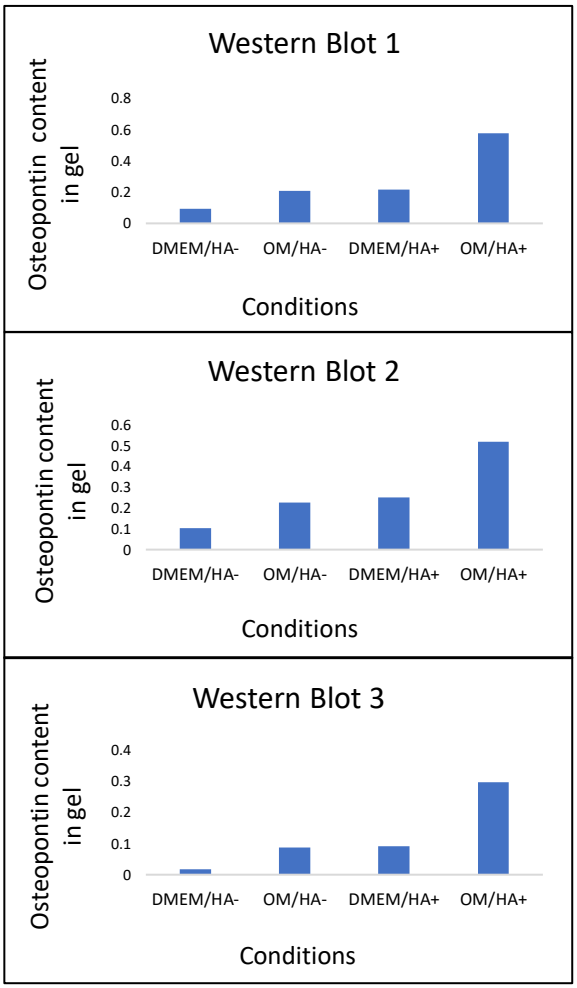

Figure 14: Quantification of the osteopontin from three experiments done

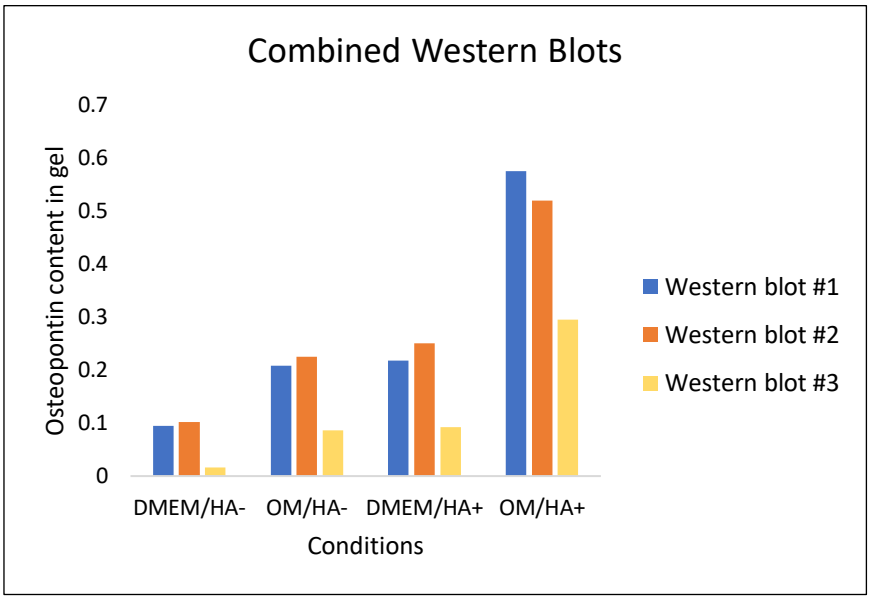

Figure 15: Visual representation of the three western blot experiments side by side

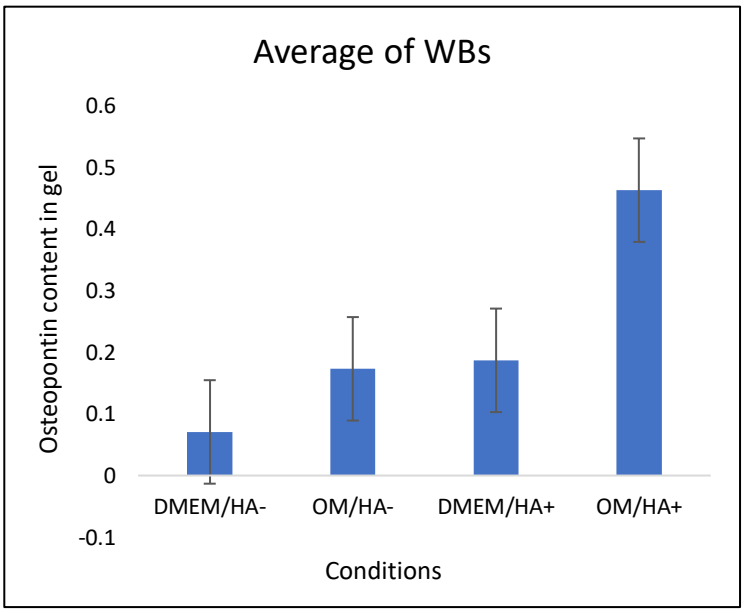

Figure 16: Average of the three western blot experiments

We can see how the osteogenic medium or the hydroxyapatite promotes a very similar osteopontin expression from these western blot figures. The absence of both promotes the least osteopontin, opposing the combination of both elements, where we can see the most osteopontin expression within our constructs, as expected.

Scanning Electron Microscope (SEM)

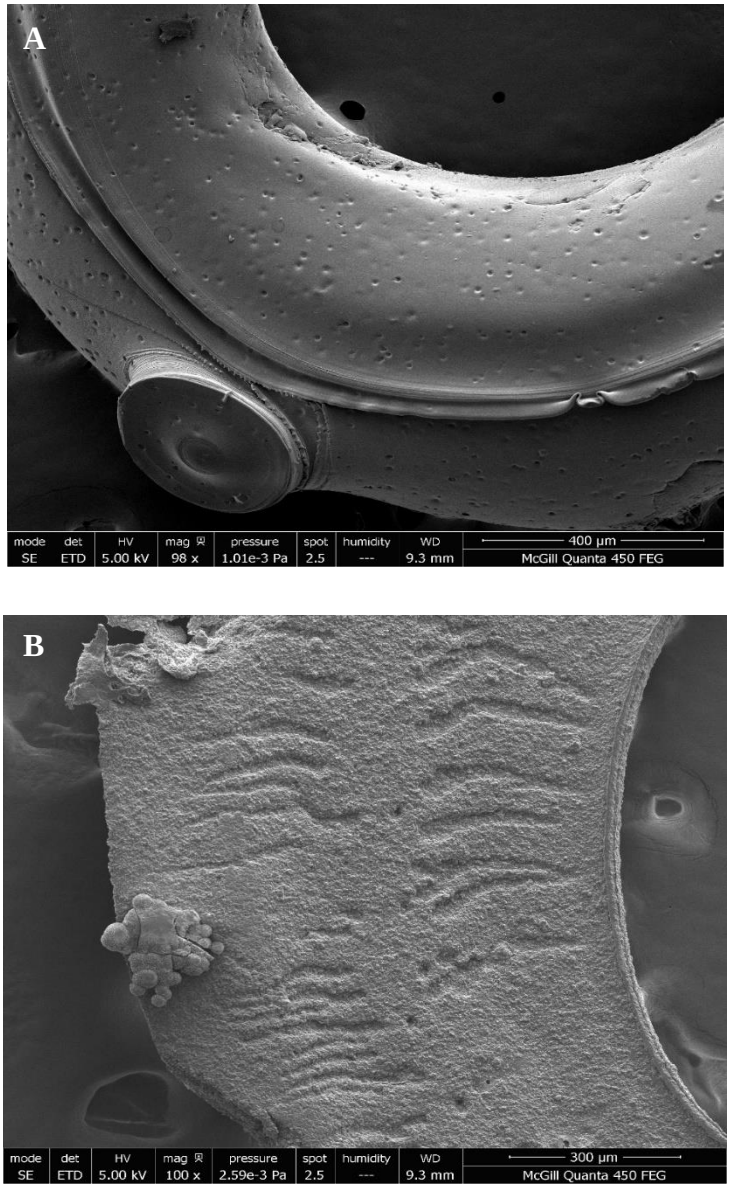

Figure 17: SEM pictures taken of two constructs at the same magnification. A) Construct without HA. B) Construct with HA.

SEM was performed at the same magnification to observe the printed constructs. Without the HA (figure 17. A), the surface topography looks pretty smooth compared to when the HA is included (figure 17. B), where it seems rougher. It is also possible to see an even distribution of the cells throughout the constructs.

Preliminary Migration Assay

A migration assay was put in place as a proof of concept to observe if the osteoblasts would react with cancer cells if put together over several days. This is a singular experiment set (n = 1), and we did not get to go any further. As we can see, over five days, when put together, the cancer cells and osteoblast seem to interact with each other by invading each other's space.

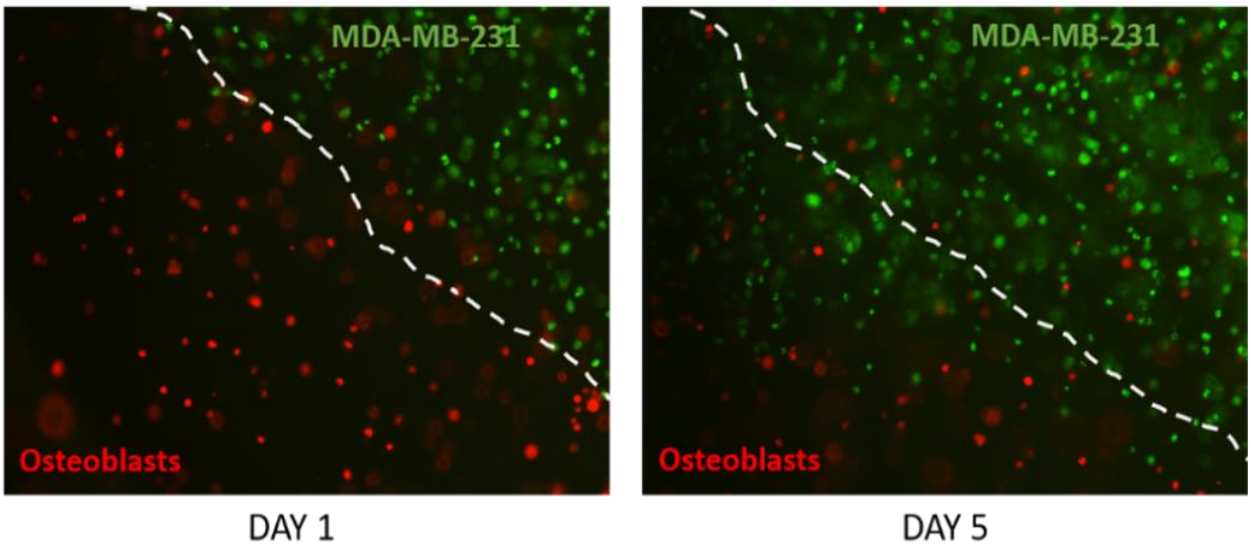

Figure 18: Migration assay performed using Deep Red labeled osteoblasts and MDA-MB-231 breast cancer cells. Pictures were taken using an Olympus IX81 inverted fluorescence microscope to monitor cell movement over five days.

DISCUSSION

Current 3D Models for Bone Environment

To date, to repair patient bone tissues, structures needed to do so are usually made in a laboratory using very high-temperature furnaces and toxic chemicals. Recently, scientists in the field developed a new technique called ceramic omnidirectional bioprinting in cell suspensions (COBICS) [121] using 3D printing technology with bioink made up of calcium phosphate, allowing them to print structures living cells that can harden very quickly. This model seems promising as the structures printed are very bone-like, the viability is high, promote osteogenesis when in close contact with the printed structures, and could be extruded directly into the patient's body after a resection caused by cancer or trauma. All things considered, this model could warrant *in situ* fabrication of bone-like structures and be employed as a drug screening tool and disease modeling.

Much like ours, this new model can be printed at room temperature, without the use of harsh chemicals or radiation. Most models that have been published in the past five years can support and maintain cells weeks after being printed. For instance, the viability of the COBICS model was monitored for 14 days with an average of 90 ± 7.0% compared to our 28 days of monitoring with an average of 87 ± 3.5%. Further, the vast majority of proposed 3D bone models use purchased human bone cells for their printed models, possibly manifesting different results seen in the human microenvironment. However, we have the privilege of being able to incorporate osteoblasts coming directly from isolated cadaveric vertebral bodies of organ donors, reproducing

results that could be seen *in vivo* with much more accuracy. Furthermore, a widespread practice in the most recent papers is the addition of human stem cells and differentiating them into bone cells via cell-specific media and performing protein analysis for osteogenesis markers and comparing the 3D constructs made by using osteoblasts differentiated from stem cells with 3D constructs made by using the human osteoblasts.

Bioprinting

For many years, scientists have tried to bridge 2D cultures to animal models. Thanks to its precise 3D geometries, 3D bioprinting has become a promising technology for *in vitro* modeling, now connecting these two. However, despite the immense progress on 3D models shown in the last decade, challenges like the lack of different cell types such as fibroblasts, endothelial cells, and immune cells make it difficult to recreate the human bone microenvironment. The lack of physical properties like fluid flow, compression, and pore size could also affect the overall representation of the human microenvironment [122]. Since bone is such a complex environment, achieving something similar will undoubtedly take many more years of work. That being said, high viability of human primary bone cells in our 3D constructs was observed within 28 days of culture. Moreover, we were able to characterize the mechanical properties of the constructs, such as stiffness. We noticed a difference between acellular constructs and cellular constructs with the addition of the primary bone mineral. The acellular constructs were smooth, while the cellular constructs with nano-hydroxyapatite were rough. Also, we demonstrated a calcified matrix secreted by osteoblasts in our model. Lastly, with the help of a protein analytical technique, the western blot, osteopontin, a major key factor in bone remodeling, was detected in our samples.

Other papers have shown different types of protein expression within their models, such as Runx2, a master transcription factor associated with osteogenesis. This avenue could be further investigated in future work.

Alginate/Gelatin Models Applications

Alginate/gelatin models have been used in different applications such as in soft tissue adhesives [123], dental tissue regeneration [124], bone healing in rat defect models [125], and multicellular tumor spheroids (MCTS) formation [118, 126]. Besides helping in the gel's flexibility, gelatin is one of the main factors responsible for cell adhesion. On the other hand, the viscous properties of the alginate provide an increase in the gel's mechanical properties. Together, they can be adjusted to seek a specific rigidity and circumvent the mechanical limitations both have individually. To benefit our system and make it a more reliable bone model for our studies, we have improved it by adding the main bone mineral, nano-hydroxyapatite. Throughout the literature, nano-hydroxyapatite is mainly documented for its restorative and regenerative applications, primarily in dentistry. Its properties include not stimulating inflammatory reactions, not being toxic to cells, and directly inducing bone growth through the osteoblasts [127-129]. We were able to implement it to our 3D printed constructs and notice the striking difference in the bone matrix between constructs that had the HA and those that did not have the HA without altering the viability of our cells. Moreover, SEM analysis shows that HA constructs seem to be stiffer than those that did not have the HA, making it a more reliable bone model.

Bone Metastasis 3D Models and the Relevancy of our Model

As of 2021, there is still a lack of extensive reports on 3D models for bone metastases in the literature. Much of the published models need to be further tested and characterized since they do not represent the entirety of the metastatic microenvironment found in clinical trials. Most seem to be only similar to the native metastatic tissues, which is expected [130], knowing the complexity of the heterogeneity found in bone metastases. However, some papers provide promising 3D models in the literature. An example of this is the *in vitro* bone matrices composed of polyethylene glycol hydrogel and nano-hydroxyapatite by Lijie Grace Zhang's team. They generated a matrix capable of embedding and maintaining breast cancer cells and osteoblasts [131]. The model is great as it can also induce cell proliferation and the secretion of cytokines that could be used to understand underlying mechanisms of bone metastasis. While 2D models offer great information on how tumor cells grow and behave to a certain extent, they cannot provide data on the complex cell-cell interactions and the tumor microenvironments [132]. However, with our 3D model, we could integrate bone cancer metastatic cells and observe them migrate as a part of our preliminary migration assay experiments over five days. It would seem that our model favors tumor cell invasion, which would realistically, in return, offer a controllable microenvironment to help further understand the metastatic process that happens in patients. Furthermore, as a potential high throughput drug screening tool, our model can serve as a platform to test the efficacy of different therapeutics on patients' cells before any therapeutic treatments may be given, which, in return, would save a lot of time and ultimately a lot of lives.

Future Directions

The next step for this project would include expanding the preliminary migration assay and establishing a pattern of migration that we can observe and understand for not only five days but weeks. Next, future work would involve adding and evaluating the effect of several different therapeutics such as doxorubicin, paclitaxel, and cyclophosphamide on cancer cells within our model. Additional work would focus on adding several types of cells into the model, such as fibroblasts, endothelial cells, and immune cells. The lack of cell diversity is one of the main drawbacks of published 3D models. We want to circumvent that to reinforce our hydrogel model's accuracy to the human bone microenvironment. Our project could take other avenues to explore the potential of bone repair and regeneration that our model could offer. Lastly, it would be interesting to put our model to test and experiment and understand primary bone cancers like sarcomas or giant cells.

CONCLUSION

To this day, no published 3D model has shown the capability to replicate the intricacy of human bone metastases fully. Understanding the complexity and heterogeneity found in bone metastases will be the key to resolve this void in the literature. The 3D bone model proposed in this thesis is adequate for printing osteoblasts and maintains high viability of cells in culture for over 28 days. This hydrogel is also able to produce bone matrix over 28 days. Osteopontin, one of the main proteins present in bone, has been detected with protein analysis, and SEM analysis shows a stiffer surface for the hydrogel embedded with HA. All in all, this model can potentially be used for modeling tissue repair regeneration as a suitable bone cancer microenvironment or as a high-throughput therapeutic screening tool.

REFERENCES

1. Su, N., et al., *Bone function, dysfunction and its role in diseases including critical illness.* International journal of biological sciences, 2019. **15**(4): p. 776-787.
2. Boskey, A.L. and A.S. Posner, *Bone structure, composition, and mineralization.* Orthop Clin North Am, 1984. **15**(4): p. 597-612.
3. Mohamed, A.M., *An overview of bone cells and their regulating factors of differentiation.* The Malaysian journal of medical sciences : MJMS, 2008. **15**(1): p. 4-12.
4. Bellido, T., *Osteocyte-driven bone remodeling.* Calcified tissue international, 2014. **94**(1): p. 25-34.
5. Feng, X., *Chemical and Biochemical Basis of Cell-Bone Matrix Interaction in Health and Disease.* Current chemical biology, 2009. **3**(2): p. 189-196.
6. Bonewald, L.F., *The Role of the Osteocyte in Bone and Nonbone Disease.* Endocrinology and metabolism clinics of North America, 2017. **46**(1): p. 1-18.
7. Tatsumi, S., et al., *Targeted ablation of osteocytes induces osteoporosis with defective mechanotransduction.* Cell Metab, 2007. **5**(6): p. 464-75.
8. Clarke, B., *Normal bone anatomy and physiology.* Clin J Am Soc Nephrol, 2008. **3 Suppl 3**(Suppl 3): p. S131-9.
9. Aarden, E.M., E.H. Burger, and P.J. Nijweide, *Function of osteocytes in bone.* J Cell Biochem, 1994. **55**(3): p. 287-99.
10. Corradetti, B., et al., *Osteoprogenitor cells from bone marrow and cortical bone: understanding how the environment affects their fate.* Stem Cells Dev, 2015. **24**(9): p. 1112-23.
11. Ohata, Y. and K. Ozono, *[Bone and Stem Cells. The mechanism of osteogenic differentiation from mesenchymal stem cell].* Clin Calcium, 2014. **24**(4): p. 501-8.
12. Czekanska, E.M., et al., *In search of an osteoblast cell model for in vitro research.* Eur Cell Mater, 2012. **24**: p. 1-17.
13. Chen, X., et al., *Osteocytogenesis: Roles of Physicochemical Factors, Collagen Cleavage, and Exogenous Molecules.* Tissue engineering. Part B, Reviews, 2018. **24**(3): p. 215-225.
14. Chen, X., et al., *Osteoblast-osteoclast interactions.* Connective tissue research, 2018. **59**(2): p. 99-107.
15. Rosenberg, N., O. Rosenberg, and M. Soudry, *Osteoblasts in bone physiology-mini review.* Rambam Maimonides Med J, 2012. **3**(2): p. e0013.
16. Goto, T., T. Yamaza, and T. Tanaka, *Cathepsins in the osteoclast.* Journal of Electron Microscopy, 2003. **52**(6): p. 551-558.
17. Caetano-Lopes, J., H. Canhão, and J.E. Fonseca, *Osteoblasts and bone formation.* Acta Reumatol Port, 2007. **32**(2): p. 103-10.
18. Patel, A., *Benign vs Malignant Tumors.* JAMA Oncol, 2020. **6**(9): p. 1488.
19. SA., F., *Dynamics of Cancer: Incidence, Inheritance, and Evolution*. Stem Cells: Tissue Renewal. Vol. Chapter 12. 2007, Princeton (NJ): Princeton University Press.
20. GM., C., *The Cell: A Molecular Approach*. 2nd edition ed. The Development and Causes of Cancer. 2000, Sunderland (MA): Sinauer Associates.
21. Greene FL, B.C., Page DL, et al, *Cancer Staging Manual*. 6th ed. 2002, New York: Springer-Verlag.
22. Kufe DW, P.R., Weichselbaum RR, et al., *Holland-Frei Cancer Medicine*. 6th ed. 2003, Hamilton (ON): BC Decker.

23. Brenner, D.R., et al., *Projected estimates of cancer in Canada in 2020.* Canadian Medical Association Journal, 2020. **192**(9): p. E199.
24. Committee, C.C.S.A., *Canadian Cancer Statistics 2019*. 2019, Canadian Cancer Society: Toronto, ON. p. 95.
25. Paget, S., *The distribution of secondary growths in cancer of the breast. 1889.* Cancer Metastasis Rev, 1989. **8**(2): p. 98-101.
26. Ribatti, D., G. Mangialardi, and A. Vacca, *Stephen Paget and the 'seed and soil' theory of metastatic dissemination.* Clin Exp Med, 2006. **6**(4): p. 145-9.
27. Gdowski, A.S., A. Ranjan, and J.K. Vishwanatha, *Current concepts in bone metastasis, contemporary therapeutic strategies and ongoing clinical trials.* J Exp Clin Cancer Res, 2017. **36**(1): p. 108.
28. Duffy, M.J., *The role of proteolytic enzymes in cancer invasion and metastasis.* Clin Exp Metastasis, 1992. **10**(3): p. 145-55.
29. Kessenbrock, K., V. Plaks, and Z. Werb, *Matrix metalloproteinases: regulators of the tumor microenvironment.* Cell, 2010. **141**(1): p. 52-67.
30. Martin TA, Y.L., Sanders AJ, et al., *Cancer Invasion and Metastasis: Molecular and Cellular Perspective. In: Madame Curie Bioscience Database [Internet].* Landes Bioscience, 2000-2013.
31. Chambers, A.F., et al., *Critical steps in hematogenous metastasis: an overview.* Surg Oncol Clin N Am, 2001. **10**(2): p. 243-55, vii.
32. Luzzi, K.J., et al., *Multistep nature of metastatic inefficiency: dormancy of solitary cells after successful extravasation and limited survival of early micrometastases.* Am J Pathol, 1998. **153**(3): p. 865-73.
33. Jayarangaiah A, T.K.P., *Bone Metastasis.* StatPearls Publishing [Internet], 2019 Jan-.
34. Ashford, R.U., et al., *The modern surgical and non-surgical management of appendicular skeletal metastases.* Orthopaedics and Trauma, 2012. **26**(3): p. 184-199.
35. Versteeg, A.L., et al., *Psychometric evaluation and adaptation of the Spine Oncology Study Group Outcomes Questionnaire to evaluate health-related quality of life in patients with spinal metastases.* Cancer, 2018. **124**(8): p. 1828-1838.
36. Aoude, A., et al., *The revised Tokuhashi score; analysis of parameters and assessment of its accuracy in determining survival in patients afflicted with spinal metastasis.* Eur Spine J, 2018. **27**(4): p. 835-840.
37. Patchell, R.A., et al., *Direct decompressive surgical resection in the treatment of spinal cord compression caused by metastatic cancer: a randomised trial.* Lancet, 2005. **366**(9486): p. 643-8.
38. Macedo, F., et al., *Bone Metastases: An Overview.* Oncol Rev, 2017. **11**(1): p. 321.
39. Coleman, R.E., *Metastatic bone disease: clinical features, pathophysiology and treatment strategies.* Cancer Treat Rev, 2001. **27**(3): p. 165-76.
40. Bauer, H.C., *Controversies in the surgical management of skeletal metastases.* J Bone Joint Surg Br, 2005. **87**(5): p. 608-17.
41. Janjan, N., *Bone metastases: approaches to management.* Semin Oncol, 2001. **28**(4 Suppl 11): p. 28-34.
42. Svensson, E., et al., *Survival after bone metastasis by primary cancer type: a Danish population-based cohort study.* BMJ Open, 2017. **7**(9): p. e016022.
43. Delank, K.S., et al., *The treatment of spinal metastases.* Dtsch Arztebl Int, 2011. **108**(5): p. 71-9; quiz 80.
44. Kuchuk, I., et al., *Incidence, consequences and treatment of bone metastases in breast cancer patients-Experience from a single cancer centre.* J Bone Oncol, 2013. **2**(4): p. 137-44.
45. Sabino, M.A. and P.W. Mantyh, *Pathophysiology of bone cancer pain.* J Support Oncol, 2005. **3**(1): p. 15-24.

46. Lipton, A., et al., *Randomized active-controlled phase II study of denosumab efficacy and safety in patients with breast cancer-related bone metastases.* J Clin Oncol, 2007. **25**(28): p. 4431-7.
47. Stopeck, A.T., et al., *Denosumab compared with zoledronic acid for the treatment of bone metastases in patients with advanced breast cancer: a randomized, double-blind study.* J Clin Oncol, 2010. **28**(35): p. 5132-9.
48. Kakhki, V.R., et al., *Pattern and distribution of bone metastases in common malignant tumors.* Nucl Med Rev Cent East Eur, 2013. **16**(2): p. 66-9.
49. Houssami, N. and C.M. Costelloe, *Imaging bone metastases in breast cancer: evidence on comparative test accuracy.* Ann Oncol, 2012. **23**(4): p. 834-43.
50. Perrin, R.G. and A.W. Laxton, *Metastatic spine disease: epidemiology, pathophysiology, and evaluation of patients.* Neurosurg Clin N Am, 2004. **15**(4): p. 365-73.
51. *The Spread of Tumours in the Human Body.* Postgraduate Medical Journal, 1953. **29**(329): p. 160-160.
52. Perrin, R.G., K.E. Livingston, and B. Aarabi, *Intradural extramedullary spinal metastasis. A report of 10 cases.* J Neurosurg, 1982. **56**(6): p. 835-7.
53. Batson, O.V., *THE FUNCTION OF THE VERTEBRAL VEINS AND THEIR ROLE IN THE SPREAD OF METASTASES.* Annals of surgery, 1940. **112**(1): p. 138-149.
54. Rogers, L. and G. Heard, *Intrathecal spinal metastases (rare tumours).* Br J Surg, 1958. **45**(192): p. 317-20.
55. Constans, J.P., et al., *Spinal metastases with neurological manifestations. Review of 600 cases.* J Neurosurg, 1983. **59**(1): p. 111-8.
56. Chin, H. and J. Kim, *Bone Metastasis: Concise Overview.* Fed Pract, 2015. **32**(2): p. 24-30.
57. Ibrahim, T., et al., *Pathogenesis of osteoblastic bone metastases from prostate cancer.* Cancer, 2010. **116**(6): p. 1406-18.
58. Zhang, H., et al., *Presentation of multiple myeloma mimicking bone metastasis from colon adenocarcinoma: A case report and literature review.* Mol Clin Oncol, 2016. **4**(1): p. 31-34.
59. van der Velden, J.M., et al., *Evaluation of effectiveness of palliative radiotherapy for bone metastases: a prospective cohort study.* J Radiat Oncol, 2018. **7**(4): p. 325-333.
60. Kirkbride, P. and I.F. Tannock, *Trials in palliative treatment--have the goal posts been moved?* Lancet Oncol, 2008. **9**(3): p. 186-7.
61. Westhoff, P.G., et al., *Quality of Life in Relation to Pain Response to Radiation Therapy for Painful Bone Metastases.* Int J Radiat Oncol Biol Phys, 2015. **93**(3): p. 694-701.
62. Laufer, I. and M.H. Bilsky, *Advances in the treatment of metastatic spine tumors: the future is not what it used to be.* J Neurosurg Spine, 2019. **30**(3): p. 299-307.
63. De Felice, F., et al., *The role of radiation therapy in bone metastases management.* Oncotarget, 2017. **8**(15): p. 25691-25699.
64. Choi, D., et al., *Spine Oncology—Metastatic Spine Tumors.* Neurosurgery, 2017. **80**(3S): p. S131-S137.
65. Dea, N., et al., *Spine Oncology – Primary Spine Tumors.* Neurosurgery, 2017. **80**(3S): p. S124-S130.
66. Autio, K.A., H.I. Scher, and M.J. Morris, *Therapeutic strategies for bone metastases and their clinical sequelae in prostate cancer.* Current treatment options in oncology, 2012. **13**(2): p. 174-188.
67. Shibata, H., et al., *Diagnosis and treatment of bone metastasis: comprehensive guideline of the Japanese Society of Medical Oncology, Japanese Orthopedic Association, Japanese Urological Association, and Japanese Society for Radiation Oncology.* ESMO open, 2016. **1**(2): p. e000037-e000037.

68. Ahangar, P., et al., *Advances in personalized treatment of metastatic spine disease.* Annals of translational medicine, 2019. **7**(10): p. 223-223.
69. Pasqualini, R. and E. Ruoslahti, *Organ targeting in vivo using phage display peptide libraries.* Nature, 1996. **380**(6572): p. 364-6.
70. Uehara, H., et al., *Effects of blocking platelet-derived growth factor-receptor signaling in a mouse model of experimental prostate cancer bone metastases.* J Natl Cancer Inst, 2003. **95**(6): p. 458-70.
71. Fidler, I.J., *The pathogenesis of cancer metastasis: the 'seed and soil' hypothesis revisited.* Nat Rev Cancer, 2003. **3**(6): p. 453-8.
72. Dolznig, H., et al., *Modeling colon adenocarcinomas in vitro a 3D co-culture system induces cancer-relevant pathways upon tumor cell and stromal fibroblast interaction.* Am J Pathol, 2011. **179**(1): p. 487-501.
73. Pickl, M. and C.H. Ries, *Comparison of 3D and 2D tumor models reveals enhanced HER2 activation in 3D associated with an increased response to trastuzumab.* Oncogene, 2009. **28**(3): p. 461-8.
74. Okawa, T., et al., *The functional interplay between EGFR overexpression, hTERT activation, and p53 mutation in esophageal epithelial cells with activation of stromal fibroblasts induces tumor development, invasion, and differentiation.* Genes & development, 2007. **21**(21): p. 2788-2803.
75. Zimmermann, M., C. Box, and S.A. Eccles, *Two-dimensional vs. three-dimensional in vitro tumor migration and invasion assays.* Methods Mol Biol, 2013. **986**: p. 227-52.
76. Breslin, S. and L. O'Driscoll, *Three-dimensional cell culture: the missing link in drug discovery.* Drug Discovery Today, 2013. **18**(5): p. 240-249.
77. Fennema, E., et al., *Spheroid culture as a tool for creating 3D complex tissues.* Trends Biotechnol, 2013. **31**(2): p. 108-15.
78. Inubushi, Y. and A. Tachibana, *Uniform spheroid formation on a laboratory-made, low cell attachment surface consisting of a chitin sheet.* Biosci Biotechnol Biochem, 2020. **84**(5): p. 997-1000.
79. Raghavan, S., et al., *Comparative analysis of tumor spheroid generation techniques for differential in vitro drug toxicity.* Oncotarget, 2016. **7**(13): p. 16948-16961.
80. Costa, E.C., et al., *Optimization of liquid overlay technique to formulate heterogenic 3D co-cultures models.* Biotechnol Bioeng, 2014. **111**(8): p. 1672-85.
81. Costa, E.C., et al., *Spheroids Formation on Non-Adhesive Surfaces by Liquid Overlay Technique: Considerations and Practical Approaches.* Biotechnol J, 2018. **13**(1).
82. Todorov, L. and T. VadeBoncouer, *Etiology and use of the "hanging drop" technique: a review.* Pain research and treatment, 2014. **2014**: p. 146750-146750.
83. Wang, S., et al., *Application of Hanging Drop Technique for Kidney Tissue Culture.* Kidney & blood pressure research, 2017. **42**(2): p. 220-231.
84. Pampaloni, F., E.G. Reynaud, and E.H.K. Stelzer, *The third dimension bridges the gap between cell culture and live tissue.* Nature Reviews Molecular Cell Biology, 2007. **8**(10): p. 839-845.
85. Bartlett, R., et al., *Personalized in vitro cancer modeling - fantasy or reality?* Translational oncology, 2014. **7**(6): p. 657-664.
86. Weiswald, L.-B., D. Bellet, and V. Dangles-Marie, *Spherical cancer models in tumor biology.* Neoplasia (New York, N.Y.), 2015. **17**(1): p. 1-15.
87. Xu, H., et al., *Organoid technology and applications in cancer research.* Journal of hematology & oncology, 2018. **11**(1): p. 116-116.
88. McCauley, H.A. and J.M. Wells, *Pluripotent stem cell-derived organoids: using principles of developmental biology to grow human tissues in a dish.* Development (Cambridge, England), 2017. **144**(6): p. 958-962.

89. Bose, B., *Induced Pluripotent Stem Cells (iPSCs) Derived 3D Human Lung Organoids from Different Ethnicities to Understand the SARS-CoV2 Severity/Infectivity Percentage.* Stem cell reviews and reports, 2021. **17**(1): p. 293-295.
90. Sung, K.E., et al., *Understanding the impact of 2D and 3D fibroblast cultures on in vitro breast cancer models.* PLoS One, 2013. **8**(10): p. e76373.
91. Chen, L., et al., *The enhancement of cancer stem cell properties of MCF-7 cells in 3D collagen scaffolds for modeling of cancer and anti-cancer drugs.* Biomaterials, 2012. **33**(5): p. 1437-44.
92. Cavo, M., et al., *Microenvironment complexity and matrix stiffness regulate breast cancer cell activity in a 3D in vitro model.* Sci Rep, 2016. **6**: p. 35367.
93. Majety, M., et al., *Fibroblasts Influence Survival and Therapeutic Response in a 3D Co-Culture Model.* PLoS One, 2015. **10**(6): p. e0127948.
94. Eder, T., et al., *Cancer-Associated Fibroblasts Modify the Response of Prostate Cancer Cells to Androgen and Anti-Androgens in Three-Dimensional Spheroid Culture.* International journal of molecular sciences, 2016. **17**(9): p. 1458.
95. Nyga, A., U. Cheema, and M. Loizidou, *3D tumour models: novel in vitro approaches to cancer studies.* J Cell Commun Signal, 2011. **5**(3): p. 239-48.
96. Vantangoli, M.M., et al., *MCF-7 Human Breast Cancer Cells Form Differentiated Microtissues in Scaffold-Free Hydrogels.* PLoS One, 2015. **10**(8): p. e0135426.
97. Harma, V., et al., *A comprehensive panel of three-dimensional models for studies of prostate cancer growth, invasion and drug responses.* PLoS One, 2010. **5**(5): p. e10431.
98. Cichon, M.A., et al., *Growth of lung cancer cells in three-dimensional microenvironments reveals key features of tumor malignancy.* Integr Biol (Camb), 2012. **4**(4): p. 440-8.
99. Ahangar, P., et al., *Current biomedical applications of 3D printing and additive manufacturing.* Applied Sciences, 2019. **9**(8): p. 1713.
100. de Vries, R., et al., *Chapter 33 - Bioengineering, biomaterials, and β-cell replacement therapy*, in *Transplantation, Bioengineering, and Regeneration of the Endocrine Pancreas*, G. Orlando, et al., Editors. 2020, Academic Press. p. 461-486.
101. Vanderburgh, J.P., S.A. Guelcher, and J.A. Sterling, *3D bone models to study the complex physical and cellular interactions between tumor and the bone microenvironment.* 2018. **119**(7): p. 5053-5059.
102. Skjåk-Bræk, G., H. Grasdalen, and O. Smidsrød, *Inhomogeneous polysaccharide ionic gels.* Carbohydrate Polymers, 1989. **10**(1): p. 31-54.
103. Andersen, T., P. Auk-Emblem, and M. Dornish, *3D Cell Culture in Alginate Hydrogels.* Microarrays (Basel, Switzerland), 2015. **4**(2): p. 133-161.
104. Abasalizadeh, F., et al., *Alginate-based hydrogels as drug delivery vehicles in cancer treatment and their applications in wound dressing and 3D bioprinting.* Journal of biological engineering, 2020. **14**: p. 8-8.
105. Sun, J. and H. Tan, *Alginate-Based Biomaterials for Regenerative Medicine Applications.* Materials (Basel), 2013. **6**(4): p. 1285-1309.
106. Lee, K.Y. and D.J. Mooney, *Alginate: properties and biomedical applications.* Progress in polymer science, 2012. **37**(1): p. 106-126.
107. Kaczmarek- Pawelska, A., *Alginate-Based Hydrogels in Regenerative Medicine*. 2019. p. 1-16.
108. He, L., et al., *Alginate-Based Platforms for Cancer-Targeted Drug Delivery.* BioMed Research International, 2020. **2020**: p. 1487259.
109. Axpe, E. and M.L. Oyen, *Applications of Alginate-Based Bioinks in 3D Bioprinting.* International Journal of Molecular Sciences, 2016. **17**(12): p. 1976.
110. Yue, K., et al., *Synthesis, properties, and biomedical applications of gelatin methacryloyl (GelMA) hydrogels.* Biomaterials, 2015. **73**: p. 254-71.

111. Gaspar-Pintiliescu, A., et al., *Physicochemical and Biological Properties of Gelatin Extracted from Marine Snail Rapana venosa.* Marine drugs, 2019. **17**(10): p. 589.
112. Sun, M., et al., *Synthesis and Properties of Gelatin Methacryloyl (GelMA) Hydrogels and Their Recent Applications in Load-Bearing Tissue.* Polymers, 2018. **10**(11): p. 1290.
113. Rose, J.B., et al., *Gelatin-Based Materials in Ocular Tissue Engineering.* Materials (Basel, Switzerland), 2014. **7**(4): p. 3106-3135.
114. Santoro, M., A.M. Tatara, and A.G. Mikos, *Gelatin carriers for drug and cell delivery in tissue engineering.* Journal of controlled release : official journal of the Controlled Release Society, 2014. **190**: p. 210-218.
115. Wang, X., et al., *Gelatin-Based Hydrogels for Organ 3D Bioprinting.* Polymers, 2017. **9**(9): p. 401.
116. Park, K.M., D. Lewis, and S. Gerecht, *Bioinspired Hydrogels to Engineer Cancer Microenvironments.* Annual review of biomedical engineering, 2017. **19**: p. 109-133.
117. Fairag, R., et al., *Three-Dimensional Printed Polylactic Acid Scaffolds Promote Bone-like Matrix Deposition in Vitro.* ACS Appl Mater Interfaces, 2019. **11**(17): p. 15306-15315.
118. Jiang, T., et al., *Directing the Self-assembly of Tumour Spheroids by Bioprinting Cellular Heterogeneous Models within Alginate/Gelatin Hydrogels.* Scientific Reports, 2017. **7**(1): p. 4575.
119. Mobasherpour, I., et al., *Synthesis of nanocrystalline hydroxyapatite by using precipitation method.* Journal of Alloys and Compounds, 2007. **430**(1): p. 330-333.
120. Denhardt, D.T., C.M. Giachelli, and S.R. Rittling, *Role of osteopontin in cellular signaling and toxicant injury.* Annu Rev Pharmacol Toxicol, 2001. **41**: p. 723-49.
121. Romanazzo, S., et al., *Synthetic Bone-Like Structures Through Omnidirectional Ceramic Bioprinting in Cell Suspensions.* Advanced Functional Materials. **n/a**(n/a): p. 2008216.
122. Kwakwa, K.A., et al., *Engineering 3D Models of Tumors and Bone to Understand Tumor-Induced Bone Disease and Improve Treatments.* Current osteoporosis reports, 2017. **15**(4): p. 247-254.
123. Yuan, L., et al., *Modified alginate and gelatin cross-linked hydrogels for soft tissue adhesive.* Artificial Cells, Nanomedicine, and Biotechnology, 2017. **45**(1): p. 76-83.
124. Yu, H., et al., *Effects of 3-dimensional Bioprinting Alginate/Gelatin Hydrogel Scaffold Extract on Proliferation and Differentiation of Human Dental Pulp Stem Cells.* J Endod, 2019. **45**(6): p. 706-715.
125. Liu, B., et al., *Cell-loaded injectable gelatin/alginate/LAPONITE® nanocomposite hydrogel promotes bone healing in a critical-size rat calvarial defect model.* RSC Advances, 2020. **10**(43): p. 25652-25661.
126. Au - Jiang, T., et al., *Bioprintable Alginate/Gelatin Hydrogel 3D In Vitro Model Systems Induce Cell Spheroid Formation.* JoVE, 2018(137): p. e57826.
127. Łabowska, M.B., et al., *A Review on the Adaption of Alginate-Gelatin Hydrogels for 3D Cultures and Bioprinting.* Materials (Basel, Switzerland), 2021. **14**(4): p. 858.
128. Pepla, E., et al., *Nano-hydroxyapatite and its applications in preventive, restorative and regenerative dentistry: a review of literature.* Annali di stomatologia, 2014. **5**(3): p. 108-114.
129. Bordea, I.R., et al., *Nano-hydroxyapatite use in dentistry: a systematic review.* Drug Metab Rev, 2020. **52**(2): p. 319-332.
130. Salamanna, F., et al., *A systematic review on in vitro 3D bone metastases models: A new horizon to recapitulate the native clinical scenario?* Oncotarget, 2016. **7**(28): p. 44803-44820.
131. Zhu, W., et al., *A 3D printed nano bone matrix for characterization of breast cancer cell and osteoblast interactions.* Nanotechnology, 2016. **27**(31): p. 315103.
132. Salamanna, F., et al., *An in vitro 3D bone metastasis model by using a human bone tissue culture and human sex-related cancer cells.* Oncotarget, 2016. **7**(47).